SPACE-TIME CORRELATIONS AND TAYLOR'S HYPOTHESIS FOR RAINFALL

A Thesis Submitted to

The Faculty of Graduate Studies and Research
of
McGill University
by
Guy Potvin

In Partial Fulfillment of the
Requirements for the Degree
of
Master of Science

Department of Physics
McGill University
Montréal, Québec
Canada
H1P 1C0

July 1993

ABSTRACT

An theoretical analysis of the space-time correlation function for rainfall and its relationship to Taylor's hypothesis is presented. The analysis assumes a homogeneous and stationary random field being advected past a fixed coordinate system with a constant velocity. Within the moving reference frame, the random field is assumed to possess quadrant symmetry. The concept of space-time isotropy is defined relative to a velocity. This is called the intrinsic velocity and represents a kinematic characteristic of the storm system apart from the advection velocity. A radial space-time correlation function is defined over a range of scales where the intrinsic velocity remains constant. The effect of the intrinsic velocity on Taylor's hypothesis is examined and an alternative is proposed. The effect of spatial resolution is evaluated theoretically on a model space-time correlation. The results from the theoretical calculation are compared with those obtained from two rain events. The radial space-time correlation functions of the rain events vary as expected with spatial resolution, but the intrinsic and advection velocities are inconclusive. The uncertainty for the intrinsic and advection velocities does not allow for a clear relationship with spatial resolution. Nor does it allow a clear determination of the effect of spatial resolution on the validity of Taylor's hypothesis. The intrinsic velocity may be approximated as constant over a certain range of time scales (15 to 70 min). Of the cases considered, the effect of the internal storm development on Taylor's hypothesis is slight. Therefore, a 'frozen turbulence' model for Taylor's hypothesis is still a good approximation.

RESUME

Une analyse théorique est présentée sur la fonction des correlations espace-temps pour la précipitation aussi bien que son effet sur l'hypothèse de Taylor. L'analyse suppose un champ aléatoire homogène et stationnaire qui subit un mouvement d'advection avec une vélocité constante par rapport à un système de coordonnées fixe. Par rapport au système de référence mobile, les correlations espace-temps du champ aléatoire sont symmetriques d'un quadrant à l'autre. Le concept d'isotropie espace-temps est défini par rapport à une vitesse. On qualifie cette vitesse d'interne et elle représente une caractéristique cinématique du système de précipitations indépendante de la vélocité d'advection. Une fonction de correlations espace-temps radiale est définie sur un domaine d'échelles où la vitesse interne est constante. L'effet de la vitesse interne sur l'hypothèse de Taylor est examiné et une meilleure alternative est formulée. L'effet de la résolution spatiale est déterminé théoriquement selon un modèle des correlations espace-temps. Les résultats théoriques sont comparés au résultats obtenus à partir de deux cas de précipitation. Les fonctions de correlation espace-temps radiales changent avec la résolution spatiale comme prévu. L'incertitude sur les vitesses internes et d'advection ne permet pas d'évaluer l'effet de la résolution spatiale sur celles-ci ni sur la validité de l'hypothèse de Taylor La vitesse interne est à peu près constante sur un domaine d'intervales de 15 à 70 minutes. L'effet du développement interne de la précipitation des cas examinés sur l'hypothèse de Taylor est minime. Un modèle de 'turbulence figée' décrit toujours d'une manière appropriée l'hypothèses de Taylor.

ACKNOWLEDGEMENTS

The author would like to acknowledge the helpfulness of all the staff at the McGill Radar Observatory. In particular, thanks are due to M. R. Duncan, F. Fabry and A. Bellon for their assistance and advice in the processing of the data, their useful and stimulating discussions, and last but certainly not least, for proof-reading this manuscript. Also, the author would like to thank I. Zawadzki for his input on the content and form of this work, as well as B. Katz and A. Kilambi for their help with the computer oriented part of the data analysis. Finally, the author would like to express his gratitude to J. Morneau for her help with the meteorological aspects of the cases analyzed.

TABLE OF CONTENTS

Abstract	i
Résumé	ii
Acknowledgements	iii
Table of contents	iv
List of figures and tables	v
List of symbols	ix
Contribution to knowledge	xii
1.Introduction	1
2. Rainfall as a random field	3
2.1. Random field theory	3
2.2. Statistics in the literature	6
3. Space-time correlations in rainfall	9
4. Spatial averaging and space-time correlations	21
5. Data analysis	28
5.1. Defining a scale	31
5.2. Defining a space-time correlation function	32
5.3. Defining a velocity	36
5.4. Results	39
6. Discussion	54
7. Conclusion	60
Appendix A : Accelerated Taylor's hypothesis	62
Appendix B : Relationship between the correlation functions	63
Bibliography	65

LIST OF FIGURES AND TABLES

FIG. 3.1. A graphic representation of equation (3.13), showing the dependence of the cut-off time for Taylor's hypothesis as a function of the velocity ratio (Vr). Note that the slope for Vr << 1 is -1, and for Vr >> 1, the curve asymptotically approaches 2. 13

FIG. 3.2. The spatial correlation function $C(\alpha) = \langle R(x+\alpha)R(x)\rangle / \langle R^2 \rangle$, obtained using 250 m resolution radar data of a convective rain event on the 19th of June, 1992. R(x) denotes rainfall rate. 14

FIG. 3.3. The same as in figure (3.2), but for a stratiform rain event on the 31st of July, 1992. Note the change in scale of the correlation axis. 14

FIG. 3.4. An illustration of the exponential Lagrangian space-time correlation function (equation (3.8)) with an intrinsic velocity of 0.4 (arbitrary units), as seen from the Eulerian frame. The advection velocity is 0.5 (arbitrary units). 16

FIG. 3.5. Power spectrum contour lines in wavenumber-frequency (k,ω) space from vertically-pointing radar reflectivity data, originally in height-time (z,t) space. Note the change in elongation with distance from the origin. 17

FIG. 4.1. The effect of spatial averaging on the spatial component of the space-time exponential correlation function, eq.(4.11). D is the length of one side of the square averaging area. 24

FIG. 4.2. The effect of spatial averaging on the temporal component of the space-time exponential correlation function, eq.(4.11). D is the length of one side of the square averaging area. 25

FIG. 4.3. The intrinsic velocities as a function of the normalized time interval for various averaging lengths (D) from the exponential Lagrangian space-time correlation function with characteristic length L and time T. 26

FIG. 5.0.1. Radar reflectivity CAPPI from a convective rain case on the 19th of June, 1992, is viewed at an altitude of 1.6 km and a resolution of 250 m. The storm system moved with a speed of approximately 40 km/hr towards the north-east. 29

FIG. 5.0.2. Radar reflectivity CAPPI from a stratiform rain case on the 31st of July, 1992, is viewed at an altitude of 2.0 km and a resolution of 250 m. The storm system moved with a speed of approximately 50 km/hr towards the north-east. 29

Table 5.0.1. McGill Radar characteristics 30

FIG. 5.3.1. The time-averaged advection velocities of the areas of rain exceeding the threshold for the rain event on the 19th of June, 1992, and on the 31st of July, 1992, using the 1 km resolution CAPPIs with no spatial averaging. 36

FIG. 5.3.2. The space-time correlations in the Eulerian frame for the rain event on the 19th of June, 1992. Notice a distinct slant due to the overall velocity. The resolution is 500 m. 37

FIG. 5.3.3. The Lagrangian space-time correlations for the convective case on the 19th of June, 1992. Note the symmetry about the 0 km axis for correlations of 0.2 or greater. The dashed line indicates the region where data is not available. 39

FIG. 5.4.1. The intrinsic velocity ($\bar{U}$), as a function of the time interval (τ_{lp}) for the convective case on the 19th of June, 1992. The 0.25, 1 and 2 km resolution CAPPIs are used for the D = 0.5, 1 and 2 km lines respectively, where D is the averaging length. 40

FIG. 5.4.2. The same as in figure (5.4.1) but for the stratiform case on the 31st of July, 1992. 40

FIG. 5.4.3. The radial space-time correlation functions for various averaging lengths (D) from the exponential space-time correlation function with characteristic length L and T (equation (4.11)). 43

FIG. 5.4.4. The radial space-time correlation functions of the convective case on the 19th of June, 1992, for various averaging lengths D. The CAPPIs have a resolution of 250 m and an altitude of 1.6 km. 45

FIG. 5.4.5. The same as in figure (5.4.4) but for the stratiform case on the 31st of July, 1992, with a resolution of 250 m and an altitude of 2.0 km. 45

FIG. 5.4.6. The same as in figure (5.4.4) for the convective case, but with a resolution of 1 km and an altitude of 3.0 km. 46

FIG. 5.4.7. The same as in figure (5.4.5) for the stratiform case, but with a resolution of 1 km. 46

FIG. 5.4.8. The same as in figure (5.4.4) for the convective case, but with a resolution of 2 km and an altitude of 3.0 km. 47

FIG. 5.4.9. The same as in figure (5.4.5) for the stratiform case, but with a resolution of 2 km. 47

FIG. 5.4.10. The intrinsic velocities of the convective case on the 19th of June, 1992, for various averaging lengths and CAPPI resolutions. The average intrinsic velocity is 11 km/hr. 48

FIG. 5.4.11. The same as in figure (5.4.10) but for the stratiform case on the 31st of July, 1992. The average intrinsic velocity is 15 km/hr. 48

FIG. 5.4.12. The same as in figure (5.4.10) but for the advection velocities. The average advection velocity is 42 km/hr. 49

FIG. 5.4.13. The same as in figure (5.4.11) but for the advection velocities. The average advection velocity is 45 km/hr. 49

FIG. 5.4.14. Characteristic times ($\rho = 1/e$) of the radial space-time correlation functions for the convective case on the 19th of June, 1992, for various averaging lengths and CAPPI resolutions. 50

FIG. 5.4.15. The same as in figure (5.4.14) but for the stratiform case on the 31st of July, 1992. 50

FIG. 6.1. The Eulerian space-time correlations for the stratiform case on the 31st of July, 1992, obtained from the 250 m resolution CAPPIs averaged to a resolution of 1 km. The CAPPIs have an altitude of 2.0 km and cover a region with a 96 km diameter. The dashed contours denote negative correlations. 54

FIG. 6.2. The Eulerian space-time correlations for the same rain event, altitude and region as in figure (6.1), but obtained from 1 km resolution CAPPIs with no averaging. The dashed contours denote negative correlations. 55

FIG. 6.3. The Eulerian temporal correlations for the case on the 31st of July, 1992, with a 2 km averaging length from the 1 km resolution CAPPIs, compared with the Eulerian spatial correlations transformed using the advection velocity (39.5 km/hr) and the modified velocity (43.5 km/hr) The intrinsic velocity is 18.3 km/hr. 57

FIG. 6.4. The cut-off times for Taylor's hypothesis divided by the maximum error (τ_c/ε_m) as a function of averaging length (D) for the convective case on the 19th of June, 1992. 58

FIG. 6.5. The same as in figure (6.4) but for the stratiform case on the 31st of July, 1992. 58

LIST OF SYMBOLS

a	Acceleration.
A	Averaging area defining the moving average for the spatially averaged rain field.
$C(\alpha, \beta, \tau)$	Correlation function between two points in space and time similar to ρ_l and ρ_e except that the mean is not subtracted from the field.
$\mathrm{Cov}(x_1, y_1, t_1, x_2, y_2, t_2)$	Covariance between two points, (x_1, y_1, t_1) and (x_2, y_2, t_2), of the rain rate in space (x,y) and time (t).
D	Averaging length where $A = D^2$.
H	Scaling exponent for the intrinsic velocity.
L	Characteristic length of the ideal exponential Lagrangian space-time correlation function.
r	Distance between two point in space, (x_1, y_1) and (x_2, y_2).
r_{st}	Dimensionless distance between two points in space-time, (x_1, y_1, t_1) and (x_2, y_2, t_2), normalized with respect to a proper space and time scale.
$R(x,y,t)$	Rain rate field at time (t) and over a horizontal plane (x,y) at a given altitude.
$R_A(x,y,t)$	Rain rate field in time (t) and over a horizontal plane (x,y) that underwent a moving spatial average centered at the point (x,y) and over an area A.
$\overline{R(x,y,t)}$	Mean rain rate as a function of time (t) and space (x,y).
$\bar{t}$	Average time from two instants (t_1) and (t_2).

T	Characteristic time of the ideal exponential Lagangian space-time correlation function.
U	Advection velocity.
$\tilde{U}$	Intrinsic velocity.
U'	Time-dependent advection velocity for an accelerated storm system.
U''	Space-time conversion factor for the modified Taylor's hypothesis, equals $\sqrt{U^2+\tilde{U}^2}$.
$\overline{U}$	Adjustment velocity which is the difference between the initial estimate of the advection velocity and the actual advection velocity.
V_r	Ratio of the intrinsic velocity ($\tilde{U}$) over the advection velocity (U)
α	Interval of space parallel to the x-axis and, by convention, the advection velocity (U).
α_e	Interval of space parallel to the x-axis with respect to the Eulerian axis.
α_l	Interval of space parallel to the x-axis with respect to the Lagrangian frame.
β	Interval of space parallel to the y-axis.
$\varepsilon(\tau)$	Error between the Eulerian time and space correlation functions as a function of the time interval.
Θ	Scale of fluctuation for a homogeneous, stationary and ergotic random field, either with respect to space ($\Theta_\alpha, \Theta_\beta, \Theta_r$) or time ($\Theta_\tau$).
Θ_c	Characteristic scale, 1/2 of the scale of fluctuation.
λ	Multiplicative scaling factor for space and time.

$\rho(x_1, y_1, t_1, x_2, y_2, t_2)$	Correlation of the rain rate between two points, (x_1, y_1, t_1) and (x_2, y_2, t_2), in space (x,y) and time (t).
$\rho_A(\alpha, \beta, \tau)$	Correlation function for a homogeneous and stationary random field (rain rate) that underwent a moving spatial average of area A.
$\rho_e(\alpha_e, \tau_e)$	Correlation function for a homogeneous and stationary random field (rain rate) with respect to the Eulerian frame.
$\rho_l(\alpha_l, \tau_l)$	Correlation function for a homogeneous and stationary random field (rain rate) with respect to the Lagrangian frame.
$\rho_l(\tau_{l\rho})$	Radial space-time correlation function in the Lagrangian frame, defined with respect to a constant intrinsic velocity.
$\sigma^2(x, y, t)$	Variance of the rain rate as a function of time (t) and space (x,y).
τ	Interval of time.
τ_c	Cut-off time beyond which Taylor's hypothesis is no longer considered valid and where the error reaches a prescibed maximum, $\varepsilon(\tau_c) = \varepsilon_m$.
τ_e	Interval of time with respect to the Eulerian frame.
τ_l	Interval of time with respect to the Lagrangian frame.
$\tau_{l\rho}$	Time interval in the Lagrangian frame corresponding to a time interval in the Eulerian frame with the same correlation value.

CONTRIBUTION TO KNOWLEDGE

To the best of the author's knowledge, this thesis contains original elements concerning the space-time structure of rainfall as well as the transformation of temporal statistics into spatial statistics. These elements are:

1. The complete structure of space-time correlations for rainfall. To the best of the author's knowledge, only purely spatial or temporal (either in the Lagrangian or Eulerian frames) correlation functions (or alternatively, power spectra) of rainfall in the horizontal plane have been analyzed to date.

2. The identification of the intrinsic velocity as a space-time characteristic internal to a storm system as well as the configuration of this velocity throughout the space-time domain analyzed. Consequently, the radial space-time correlation functions are defined and measured for the first time.

3. The limits imposed by the internal space-time correlation function on the validity of Taylor's hypothesis and the reformulation of Taylor's hypothesis by incorporating the internal storm space-time characteristics.

P. S.: After submitting this thesis, the author discovered the work of Nakamoto et al. (1990), who obtained space-time correlations for rainfall with different methods and goals.

1. Introduction

In 1938, G. I. Taylor examined the behavior of a turbulent stream of air where the mean velocity of the flow is much greater than the characteristic velocity of the eddies. He assumed that these eddies did not change appreciably during their passage through a wind tunnel. In this way, the velocity fluctuations observed at a given point over time are comparable to the fluctuations at a given time over space. Therefore, the temporal data may be transformed into spatial data, and vice versa, using the mean velocity as a conversion factor. This simple relationship between space and time is known as Taylor's hypothesis, and although much progress has been made in the theory of turbulence since then, interest in this hypothesis has remained (Heskestad, 1965, and Antonia et al., 1980). The reason is mainly practical, since it is easier to obtain high resolution temporal data at a given place than high resolution spatial data. Taylor's hypothesis is then the simplest way of extracting spatial information from a time series.

The same problem occurs in meteorological data, much of it consisting of time series of quantities such as temperature, pressure or rainfall, at a given place. Until the 1950s, the raingage was the principal instrument for measuring rainfall. But with radar, observing rainfall in time and over space, the validity of Taylor's hypothesis may be evaluated in a practical way (Zawadzki 1973a, Lachapelle 1990). The objective here is to develop a general framework for describing space-time correlations in rainfall, and to evaluate Taylor's hypothesis within this framework. The focus is on particular rain events, where an advection velocity often exists which is approximately constant. Such a velocity is a necessary first step towards defining Taylor's hypothesis because it serves as a basis for the space to time conversion. This basis is independent of the details of the phenomenon under study, be it turbulence or rainfall, if we assume that the phenomenon and the advection are, to first order, uncoupled. Corrections to this space to time conversion factor can be included as a second order effect, depending on the characteristics of the advected phenomenon as well as a possible relation between it and its advection. Such an approach was undertaken for turbulence by Wyngaard and Clifford (1977), and for rainfall by Waymire et al. (1984) and by Gupta and Waymire (1987). In this work, we shall introduce a velocity which characterizes the internal development of a storm system. Taylor's hypothesis can be evaluated and modified on the basis of this velocity along with the advection velocity.

We shall start by reviewing the theory of random fields and their place in the meteorological literature in section 2. Then, in section 3, we examine in theory the effect of certain symmetry assumptions about the rainfall field on its space-time correlation structure and Taylor's hypothesis. In section 4, we see the effect of spatial resolution on the space-time correlation function. This is important mainly because radar has a resolution which varies with range and the rain field has many scale-dependent properties. Therefore, we must know its effect in order to properly interpret the results. Finally in section 5, we examine the results from real data, compare them with a numerical simulation and assess their meaning. It is hoped that this work will give a greater understanding of the statistics of rainfall and help in the interpretation of temporal data, such as from raingages or vertically-pointing radar.

2. Rainfall as a random field

To make a statistical analysis of precipitation patterns, one must specify the assumptions used in the analysis and in the interpretation of the results. Normally, statistics refer to the properties of a set of independent realizations. In the case of rainfall patterns, one would need an entire series of storm events which are independent yet similar enough to count as different realizations of the same synoptic situation. This is very impractical. Fortunately, there are certain simplifying assumptions. These are homogeneity, stationarity and ergodicity. These notions are defined in the next section.

2.1. Random field theory

We begin by introducing some of the theory of random fields. A random field is just like a random variable except that instead of a number, we have a field in n-dimensional space as the outcome of any given trial or realization. The term 'realization' refers to the determination of one possibility out of many possibilities. The result of a coin toss is a realization; the choice of one possibility from two equally likely possibilities. In this case, we have a scalar field (rainfall) in two spatial dimensions and one temporal dimension. Put another way, we have $R_i = R_i(x, y, t)$, where i is an index identifying one particular realization out of all possible realizations. Here we assume that i is discrete and that the set of all possible realizations is countable. For every realization i, we attribute a probability P_i. From this, we can define the mean field, by summing over the possible realizations multiplied by their respective probabilities, as

$$\overline{R(x,y,t)} = \sum_{i=1}^{N} P_i R_i(x,y,t) \tag{2.1.1}$$

the variance as

$$\sigma^2(x,y,t) = \sum_{i=1}^{N} P_i [R_i(x,y,t) - \overline{R(x,y,t)}]^2 \tag{2.1.2}$$

the covariance between two points $(x_1, y_1, t_1), (x_2, y_2, t_2)$ as

$$\mathrm{Cov}(x_1, y_1, t_1, x_2, y_2, t_2) = \sum_{i=1}^{N} P_i [R(x_1, y_1, t_1) - \overline{R(x_1, y_1, t_1)}]\,[R(x_2, y_2, t_2) - \overline{R(x_2, y_2, t_2)}] \tag{2.1.3}$$

and the correlation between two points as

$$\rho(x_1, y_1, t_1, x_2, y_2, t_2) = \frac{\mathrm{Cov}(x_1, y_1, t_1, x_2, y_2, t_2)}{\sqrt{\sigma^2(x_1, y_1, t_1)\sigma^2(x_2, y_2, t_2)}} \tag{2.1.4}$$

where $\rho(x_1, y_1, t_1, x_1, y_1, t_1) = 1$ by definition.

Another useful concept is that of the ensemble. An ensemble is a set containing an infinite number of identically prepared systems, each independent from the others. This set allows us to define the mean, variance, covariance and correlation fields, assuming they exist, simply by averaging over the ensemble. The probabilities P_i can be interpreted as the relative frequency with which $R_i(x, y, t)$ appears in the ensemble.

Stationarity refers to statistics that are constant in time and homogeneity to statistics that are constant in space. If we have both, this means $\overline{R(x, y, t)} = \overline{R}$ and $\sigma^2(x, y, t) = \sigma^2$. Also, if the statistics are the same over time and space then no particular point is privileged. Therefore, only intervals of time and space matter for the two point functions. In other words,

$$\mathrm{Cov}(x_1, y_1, t_1, x_2, y_2, t_2) = \mathrm{Cov}(x_2 - x_1, y_2 - y_1, t_2 - t_1) \tag{2.1.5}$$

and the same applies for the correlation function. Isotropy refers to statistics that do not change with respect to direction, i.e.

$$\mathrm{Cov}(x_1, y_1, t_1, x_2, y_2, t_2) = \mathrm{Cov}(r, t_2 - t_1) \tag{2.1.6}$$

$$\text{where } r = \sqrt{(x_2 - x_1)^2 + (y_2 - y_1)^2}$$

is isotropic as well as homogeneous. Note that isotropy refers only to space and that one cannot readily extend this notion to space and time since we are dealing with two physically different quantities. Ergodicity refers to a stationary and/or homogeneous random field where a single realization that is sufficiently large contains enough statistical information to reliably estimate the ensemble mean, variance and covariance. For example, if we have an ergodic one-dimensional random field such as a time series, we need only collect data for a long time and average over time to estimate the ensemble mean.

From the correlation function we can define a correlation length (or decorrelation length, the two terms are used interchangeably), which is how far apart two points in a random field must be before they can be considered independent. For example, let us consider a stationary time series with a correlation function $\rho(\tau)$, where $\tau = t_2 - t_1$. The scale of fluctuation is defined as (Vanmarcke 1983)

$$\Theta = \int_{-\infty}^{\infty} \rho(\tau)d\tau = 2\int_{0}^{\infty} \rho(\tau)d\tau \tag{2.1.7}$$

and the characteristic scale is (Gupta & Waymire 1987)

$$\Theta_c = \int_{0}^{\infty} \rho(\tau)d\tau \tag{2.1.8}$$

where $\Theta = 2\Theta_c$. If the integrals diverge then a scale does not exist. One condition necessary for its existence is

$$\tau\rho(\tau) = 0, \text{ as } |\tau| \to \infty \tag{2.1.9}$$

The correlation function may approach a power law for large τ (i.e. $\rho(\tau) \to |\tau|^{-\alpha}$, for $|\tau| \to \infty$), in which case the scale of fluctuation exists if $\alpha > 1$. If the scale of fluctuation exists and if the time interval of observation is T, then the ratio T/Θ can be interpreted as the equivalent number of independent observations in the sample (Vanmarcke 1983). The characteristic scale has certain advantages when dealing with an exponential correlation function $\rho(\tau) = \exp(-|\tau|/T)$ because $\Theta_c = T$. In fact, the characteristic scale is sometimes defined as the point where $\rho(\Theta_c) = e^{-1}$ whether or not the correlation function is exponential. This is done in a context where the correlation function can always be approximated as an exponential and the integration is problematical. We can extend these definitions to include many dimensions,

$$\Theta_\tau = \int_{-\infty}^{\infty} \rho(0,0,\tau)d\tau \tag{2.1.10}$$

$$\Theta_\alpha = \int_{-\infty}^{\infty} \rho(\alpha,0,0)d\alpha \tag{2.1.11}$$

$$\Theta_\beta = \int_{-\infty}^{\infty} \rho(0,\beta,0)d\beta \tag{2.1.12}$$

where, $\alpha = x_2 - x_1$ and $\beta = y_2 - y_1$. For isotropy,

$$\Theta_r = 2\int_{0}^{\infty} \rho(r,0)dr = \Theta_\alpha = \Theta_\beta \tag{2.1.13}$$

2.2. Statistics in the literature

Ergodicity has been suggested by Atlas et al. (1990) for convective rainfall. They argued that convective cells have a quasi-deterministic development. That is the rain rate for a given cell evolves in a deterministic manner which is modulated by a random component. This is because the maximum rain rate R in a storm cell is determined by the maximum updraft and the vertical gradient of saturation vapor density (Adler and Mack 1984), along with the maximum parcel convective energy (Zawadzki and Ro 1978). During the cell's lifetime, the updraft and the rain rate will evolve in a more or less deterministic manner. Added to this is the effect of turbulent eddies which enhance or inhibit the local rain rate due to a combination of entrainment, growth or evaporation, and convergence. Furthermore, since the intensity of turbulence is controlled mainly by the horizontal shear of the vertical velocity, turbulence is proportional to the strength of the updraft. And since turbulence causes the random part of the distribution of R, we can expect the variance of the probability density function (pdf) to vary with the mean (Short and North 1990, also Zawadzki 1973a). In the case of a storm, we usually have many cells clustered together. The cells in the cluster intensify and decay throughout the cluster's history. So at any moment there are many cells at various stages of development, especially if there are many clusters in view. Therefore, provided that the evolution of the cells are not synchronous, the instantaneous realization of a rain field should give a good approximation of the pdf. Assuming, of course, that the distribution of rain rate within a cell and over its lifetime, dominate the overall pdf of rain. In this sense the field is ergodic and the statistics over space of a realization can yield the ensemble at a given point. Note that the statistics obtained in this context refer only to the processes occurring within the predominating synoptic conditions over the region and interval of time of observation. However, the work by Drufuca (1977), where the pdf taken from a raingauge over ten years coincides with the pdf obtained from radar data on patterns of intense precipitation over a wide region but one summer. Although this coincidence is strongest between 10 mm/hr and 100 mm/hr and decreases for higher rain rates, and that the radar data was calibrated with respect to the raingage data, it implies nevertheless a weak form of ergodicity that extends to many synoptic conditions. This may imply that the pdf is dominated by cells which do not change very much from one synoptic condition to another.

A rain field also consists of regions with and without precipitation. Even if we assume that the rainfall within a precipitating region is ergodic in time and space, there remains the question of the statistics of the size, shape and position of these regions. For example, Crane (1990) states that for a 256x256 km^2 region with 1 km resolution, the cumulative distribution of rain rate may be approximated by a lognormal distribution above the median rain rate when more than 10% of that region is covered by rainfall. This supports the assumption of ergodicity within precipitating regions. A lognormal distribution appears often in the literature, not only for rain rate but other quantities as well. Indeed, Rosenfeld et al. (1990) show lognormal distributions for rain rate and Biondini (1976) found evidence for a lognormal distribution of the rain volume, lifetime and intensity of rain from Florida cumulus clouds, followed by Lopez (1976, 1977) who demonstrated a lognormal frequency distribution of height, horizontal size and duration of cloud and radar echo populations. As for the size of precipitating regions, one study by Dennis & Fernald (1963) suggests that the frequency distribution as a function of radius of isolated showers is exponential, with the characteristic radius varying with time and place.

Atmospheric fields can also exhibit scale invariant behaviour. This means that cloud or rain fields are similar from one scale to another, relative to a scale changing transformation. The scale change transformation is normally a power-law involving the ratio of a quantity from the field itself (such as the absolute value of the difference in rain rate between two points a certain distance apart or the spatial average of the rain rate over a square with a certain side length) at two different scales and the ratio of the scales themselves. Fields that display such behaviour are normally qualified as scaling or self-similar. Early work on scaling fields dealt with patterns in cloud or rain fields that are fractal, essentially geometric shapes that are scaling, either exactly or statistically. Lovejoy (1982) showed that the perimeter of a cloud or rain area is proportional to the square root of its area raised to the power of D, where $D = 1.35$ and is known as the fractal dimension of the perimeter. The consistency of this relationship from length scales ranging from 1 to 1000 km indicates the absence of a characteristic length scale within this range. The area-perimeter relationship was later explained theoretically in terms of turbulent diffusion by Hentschel & Procaccia (1984). However, Cahalan and Joseph (1989) subsequently found different dimensions for different cloud types as well as a break in the scaling behaviour of cloud base areas at a diameter of approximately 2 km. This line of investigation reached its peak with the formulation of a fractal model for rain (Lovejoy and Mandelbrot 1985, Lovejoy and Schertzer 1985).

Fractal models of rainfall were eventually supplanted by multifractal models (Schertzer and Lovejoy 1987, Lovejoy and Schertzer 1990, 1992, Tessier et al. 1993). Multifractals apply to scalar fields with no negative values (i.e. a 'mass' distribution) and so are well suited for treating rainfall. They can be thought of as fields where the geometric shapes created by the exceedence sets over a given threshold value have fractal dimensions which vary as a function of the threshold value, though this is somewhat of an over-simplification. Closely related to multifractals are multiplicative cascades (Shertzer and Lovejoy 1987, Gupta and Waymire 1993).

A multiplicative cascade is a stochastic process where an initial 'mass' is uniformly distributed over an area and subsequently redistributed to smaller areas contained in the original area, where the redistribution is done by multiplying the original 'mass' by a random variable for each sub-area. These random variables are independent and identically distributed for each sub-area. This operation is then repeated for each sub-area into even smaller sub-areas and so on, until a minimum scale is reached. These types of processes often give rise to multifractal fields. An equivalent picture to that of multifractals is expressed as multiscaling (Seed 1989, Gupta and Waymire 1990) which refers to the different scaling properties of the different moments of the spatially averaged rainfall probability distributions, with respect to the size of the averaging area. Here, no explicit reference to multifractal dimensions is made.

The relevance of the above discussion on this work has to do with the notion of ergodicity and the form of the correlation function. It has been demonstrated that a power-law form of the correlation function can arise in multifractal (Cates and Deutsch 1987) and even simple scaling fields (Waymire 1985). And from equation (2.1.9), a characteristic scale may not exist depending on the value of the exponent of the power-law, thus placing the notion of ergodicity in jeopardy. On the other hand, there is empirical evidence showing the existence of an exponential form of the correlation function from Zawadzki (1973a, 1987) and Drufuca and Zawadzki (1975). We shall therefore rely on those results and the arguments of Atlas et al. (1990) when analyzing the space-time correlations of the cases presented.

3. Space-time correlations in rainfall

Storm systems are very often advected past the region where they are observed. For the Montreal region within the range of the radar (200km), the velocity of a given storm system can be approximated as constant over the duration of the event for most cases. It is therefore possible to define an Eulerian reference frame, that is, a coordinate system fixed to the ground, and a Lagrangian reference frame which moves along with the storm system. If we treat the storm system as a homogeneous and stationary random field, then in the Lagrangian frame we can expect quadrant symmetry to hold for the space-time correlation function. In other words we expect

$$\rho_l(\alpha_l, \tau_l) = \rho_l(-\alpha_l, -\tau_l) \tag{3.1.a}$$

$$\rho_l(\alpha_l, \tau_l) = \rho_l(-\alpha_l, \tau_l) \tag{3.1.b}$$

$$\rho_l(\alpha_l, \tau_l) = \rho_l(\alpha_l, -\tau_l) \tag{3.1.c}$$

where α_l is a spatial interval in the Lagrangian frame, τ_l is a time interval in the Lagrangian frame and $\rho_l(\alpha_l, \tau_l)$ is the space-time correlation function. The correlation function should have two spatial dimensions but one was omitted from the notation for the sake of simplicity. Physically speaking, when we focus on the Lagrangian frame we eliminate the overall motion of the storm caused by large scale forcing and concentrate on the smaller scale activity of the storm. The first property, equation (3.1.a), holds by definition of the correlation function for a stationary and homogeneous field. The second property, equation (3.1.b), holds for a random space-time field with no mean motion. That is, over the entire ensemble of space-time realizations the average motion of any distinguishable feature is zero. Therefore we only need the region $0 \le \alpha_l < \infty$, $0 \le \tau_l < \infty$ to determine the entire space-time correlation function. The third property, equation (3.1.c), holds by virtue of the first and second properties.

If the storm system is advected with a constant velocity U, we have the Galilean transformation

$$\alpha_e = \alpha_l + U\tau_l \tag{3.2.a}$$

$$\tau_e = \tau_l \tag{3.2.b}$$

where α_e, τ_e are the space and time intervals in the Eulerian frame respectively. Again, the second spatial dimension has been omitted and the velocity is assumed to be parallel to the space intervals. From eq. (3.2.b) we can see that the Lagrangian and Eulerian time intervals are the same, so we drop the subscripts when referring to them. Therefore, the relation between the Eulerian and Lagrangian space-time correlation is

$$\rho_e(\alpha_e,\tau) = \rho_l(\alpha_e - U\tau,\tau) \tag{3.3}$$

So the function $\rho_e(\alpha_e,\tau)$ is symmetric about the line $\alpha_e - U\tau = 0$. By symmetric, we mean that $\rho_e(U\tau - \Delta\alpha_e,\tau) = \rho_e(U\tau + \Delta\alpha_e,\tau)$ for any τ and $\Delta\alpha_e$. Taylor's hypothesis states

$$\rho_e(0,\tau) = \rho_e(U\tau,0) \tag{3.4}$$

which, if it holds, is a way of finding the spatial correlation function from the temporal correlation function (or vice versa) using the advection velocity. This was the original form for Taylor's hypothesis (Taylor 1938) and is essentially a statistical statement about temporal and spatial data. While the model of 'frozen turbulence', that is a spatial pattern that does not evolve with time but is advected past a point with a constant velocity U, leads to equation (3.4), the reverse is not necessarily true. Other versions of Taylor's hypothesis deal with the relationship between time and space derivatives (Heskestad 1965). However, the extent to which Taylor's hypothesis allows temporal data to be transformed directly into spatial data using a velocity is not clear. We shall deal exclusively with the statistical version of Taylor's hypothesis described in equation (3.4).

Equation (3.4) also means

$$\rho_l(U\tau,\tau) = \rho_l(U\tau,0) \tag{3.5}$$

Therefore, given a Lagrangian space-time correlation function, not only can we determine the validity of Taylor's hypothesis using the value of the advection velocity of that particular case, but also for any other value. This assumes, of course, that there is no correlation between the structure of the Lagrangian space-time correlations and the advection velocity.

It sometimes happens that the advection velocity contains a small but persistent acceleration that cannot be ignored without biasing the statistics. Fortunately, this nonstationarity can be taken into account in an accelerated form of Taylor's hypothesis. The transformation from Eulerian to Lagrangian correlation is now

$$\rho_e(\alpha_e, \tau, \bar{t}) = \rho_l(\alpha_e - (U_0 + a\bar{t})\tau, \tau) \tag{3.6}$$

where $\bar{t}$ is the time in the middle of the interval τ, U_0 is the velocity at time $t = 0$, and a is the acceleration. For a complete derivation of this result, see appendix A. Therefore, if we keep $\bar{t}$ constant, we can define a new velocity $U' = U_0 + a\bar{t}$ and retrieve the old transformation

$$\rho_e(\alpha_e, \tau) = \rho_l(\alpha_e - U'\tau, \tau) \tag{3.7}$$

So in an accelerated system, we can define a local Taylor's hypothesis about an average time $\bar{t}$ where the advection velocity is a linear function of $\bar{t}$.

It would be instructive to see the effect of a Lagrangian space-time correlation structure on the validity of Taylor's hypothesis for a simple case. Let us use the Lagrangian space-time correlation function,

$$\rho_l(\alpha_l, \tau) = \exp - \left(\left(\frac{\alpha_l}{L} \right)^2 + \left(\frac{\tau}{T} \right)^2 \right)^{\frac{1}{2}} \tag{3.8}$$

which, from now on, shall serve as a simple comparative model. A form similar to this was given by Zawadzki (1975), although it implicitly assumed the validity of Taylor's hypothesis. We also define an error on Taylor's hypothesis as

$$\varepsilon(\tau) = \left| \frac{\rho_e(0,\tau) - \rho_e(U\tau, 0)}{\rho_e(0,\tau) + \rho_e(U\tau, 0)} \right| \tag{3.9}$$

provided the denominator does not vanish. By replacing the Eulerian space-time correlation with the Lagrangian, the error becomes,

$$\varepsilon(\tau) = \left| \frac{\rho_l(U\tau,\tau) - \rho_l(U\tau, 0)}{\rho_l(U\tau,\tau) + \rho_l(U\tau, 0)} \right| \tag{3.10}$$

Now, substituting the space-time correlation function of equation (3.8) into equation (3.10) and after some manipulation, we obtain

$$-\ln\left(\frac{1+\varepsilon(\tau)}{1-\varepsilon(\tau)} \right) = \left\{ 1 - \sqrt{1 + \left(\frac{L}{TU} \right)^2} \right\} \frac{U\tau}{L} \tag{3.11}$$

In the work by Zawadzki (1973a), a cut-off time was observed for Taylor's hypothesis in rainfall. This cut-off time was the maximum time interval over which Taylor's hypothesis is reasonably valid. Assuming the error is a monotonically increasing function of the time interval, which is the case here, we can define a unique cut-off time τ_c when the error attains the maximum tolerance $\varepsilon(\tau_c) = \varepsilon_m$. If the error is not monotonically increasing with the time interval then many intervals may have the maximum error value. In which case the smallest interval is taken as the cut-off time. In addition, we define an intrinsic velocity $\tilde{U} = L/T$ which characterizes the internal activity of the storm system rather than an advection. The physical significance of this velocity is not obvious. A high value of the intrinsic velocity may characterize a more active storm than a low value because, given a feature of size L, a short characteristic time would imply more activity than a long one. But supercell thunderstorms have cells of comparatively small size which can persist for hours, thus suggesting a low intrinsic velocity, and yet they are very active. Perhaps a better interpretation would be as a measure of the persistence of features of size L. In this sense, the intrinsic velocity characterizes the internal kinematic features of the storm rather than dynamic ones. Put in another way, the intrinsic velocity is a space-time conversion factor which allows temporal correlations to be converted into spatial correlations in the Lagrangian frame. It defines a Lagrangian Taylor's hypothesis, one which is inherent to the storm and does not depend on any actual motion.

Finally, placing all these elements in the previous equation and assuming that $\varepsilon_m \ll 1$ so we can expand the natural logarithm as a power series and keep only the first term, we obtain

$$-2\varepsilon_m = \left\{1 - \left[1 + \left(\frac{\tilde{U}}{U}\right)^2\right]^{\frac{1}{2}}\right\}\left(\frac{U}{\tilde{U}}\right)\left(\frac{\tau_c}{T}\right) \tag{3.12}$$

Isolating τ_c and defining a velocity ratio $V_r = \tilde{U}/U$ yields

$$\tau_c = \frac{2\varepsilon_m V_r T}{\sqrt{[1 + V_r^2]} - 1} \tag{3.13}$$

Here we have the effect of the internal development of a storm system and its advection velocity on the validity of Taylor's hypothesis summed up in one equation. For a "frozen" spatial rainfall pattern, i.e. a spatial pattern that is constant with time in the Lagrangian frame, which is advected with a fixed velocity U, the temporal scale $T \to \infty$, the velocity ratio $V_r \to 0$ and it is not difficult to verify that $\tau_c \to \infty$, as expected. If the rainfall pattern is not frozen but is advected very rapidly, such that $V_r \ll 1$, then by expanding the square root as a power series and by neglecting the second and higher order terms, we obtain $\tau_c \approx (4\varepsilon_m/V_r)T$. Which if we postulate $V_r \ll 4\varepsilon_m$ gives $\tau_c \gg T$. Inversely, if we postulate $V_r \gg 1$ and approximate using power series again, we find that $\tau_c \approx 2\varepsilon_m T$, or $\tau_c \ll T$. These conclusions probably hold for many of the space-time correlation functions of the form $\rho_l(\alpha_l, \tau) = \rho_l(r_{st})$, where $r_{st}^2 = (\alpha_l/L)^2 + (\tau/T)^2$ is a dimensionless space-time distance. Figure (3.1) shows a plot of equation (3.13) with the cut-off time normalized by $(\varepsilon_m T)$. If the intrinsic velocity, characteristic time and the error are assumed constant, then figure (3.1) shows the relation between the cut-off time and the inverse of the advection velocity given a non-zero intrinsic velocity.

Simulated cut-off time

FIG. 3.1. A graphic representation of equation (3.13), showing the dependence of the cut-off time for Taylor's hypothesis as a function of the velocity ratio (Vr). Note that the slope for Vr << 1 is −1, and for Vr >> 1, the curve asymptotically approaches 2.

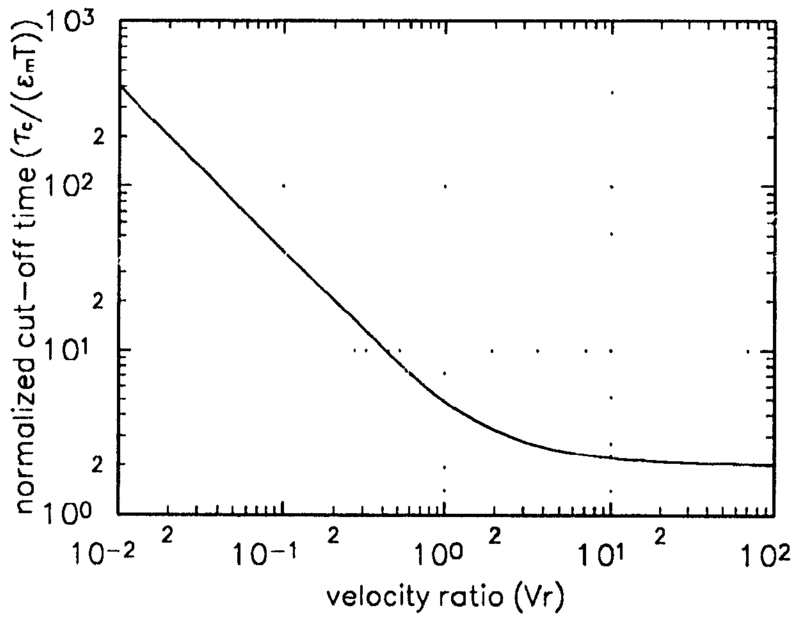

Incidentally, the motivation for studying this form comes from the fact that the correlation functions for rainfall, spatial as well as temporal, often resembles an exponential, as shown by Zawadzki (1973a), Drufuca & Zawadzki (1975), as well as by figures (3.2) and (3.3). Also, the space-time correlation function in equation (3.8) is not separable, the definition and importance of which will be made clear in the next section. It has been suggested (Mejía & Rodríguez-Iturbe 1974, Rodríguez-Iturbe & Mejía 1974a) that the two-dimensional correlation function should have the form $r_{st}K_1(r_{st})$, where K_1 is a modified Bessel function. This is based on the work by Whittle (1954), which shows that in a two-dimensional plane the Bessel function

FIG. 3.2. The spatial correlation function $C(\alpha) = \langle R(x+\alpha)R(x)\rangle / \langle R^2\rangle$, obtained using 250 m resolution radar data of a convective rain event on the 19th of June, 1992. $R(x)$ denotes rainfall rate.

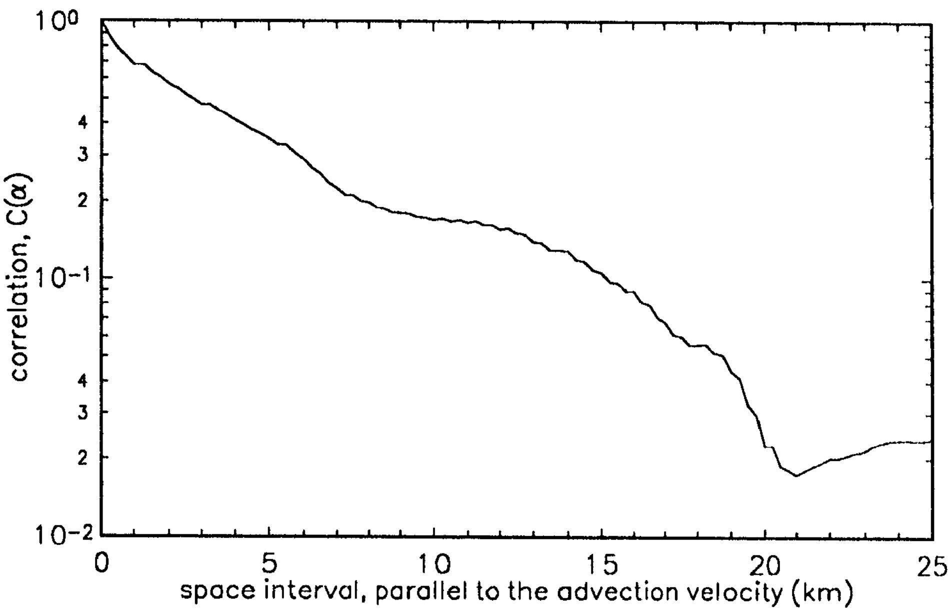

FIG. 3.3. The same as in figure (3.2), but for a stratiform rain event on the 31st of July, 1992. Note the change in scale of the correlation axis.

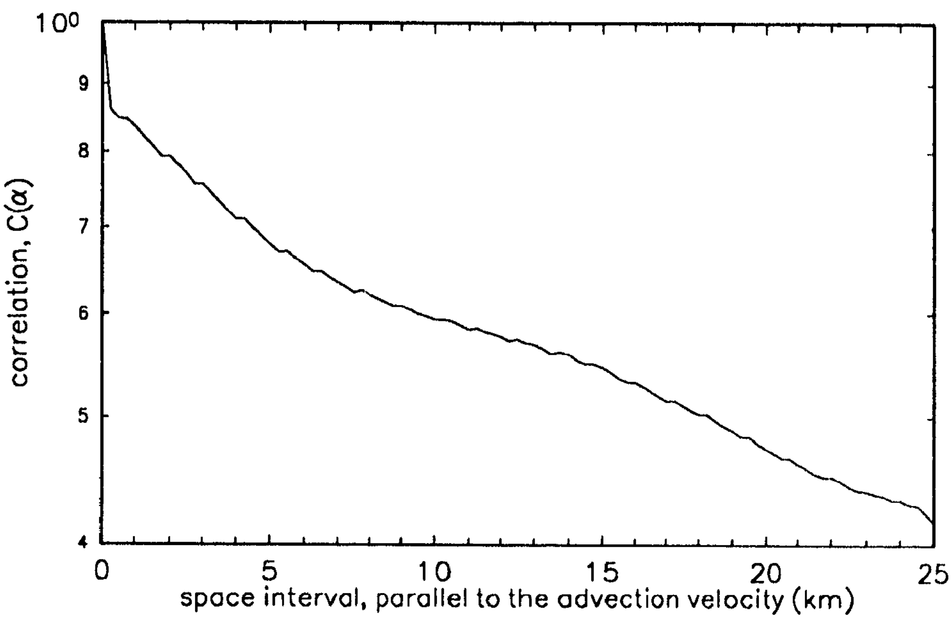

correlation can be obtained from a much simpler stochastic process than the exponential. The difference between the two is slight, however, and so we will not make such fine distinctions here.

An explanation for figures (3.2) and (3.3) is needed. Note that the correlation function used, $C(\alpha) = \langle R(x+\alpha)R(x)\rangle / \langle R^2 \rangle$, where $\langle\,\rangle$ signifies averaging over the entire space-time domain, is not the one shown in equation (2.1.4) since the mean is not subtracted from the rain field. This form of correlation was first used for rainfall by Zawadzki (1972) and has the property of never being negative, which is convenient in logarithmic plots. It is also well suited for studying the possible multifractal nature of rain (see section 2.2). Authors such as Cates and Deutsch (1987), Siebesma and Pietronero (1988), Meneveau and Chhabra (1990) and Lee and Halsey (1990) have shown that multifractals produced by discrete multiplicative cascades have power-law correlation functions of the form (to within a multiplicative constant) $C(\alpha) = (\alpha/r)^{-b}$, where b is some positive exponent, r is an inner scale of the cascade process below which the field is uniform. For multifractal fields, the mean is not subtracted from the field before the correlation is determined. That is why it was not done here, so that any power-law behaviour in the correlation would not be obscured by such an operation.

An illustration of the previous discussion can be seen in figure (3.4). In it, we see the Lagrangian space-time correlation function described in equation (3.8) advected with a velocity $U = 1/2$ (arbitrary units), as seen in the Eulerian frame. The Eulerian time correlations are the correlations along the line $\overline{OA}$, where point O denotes the origin. The Lagrangian time correlations are along the line $\overline{OB}$. Note that due to the Galilean transformation (equations (3.2.a-b)), the Lagrangian time interval, $\overline{OD}$, is the same as the Eulerian time interval, $\overline{OC}$. The intrinsic velocity is $\tilde{U} = 0.4$ and it corresponds to the ratio of the space interval $\overline{OE}$ over the corresponding Lagrangian time interval, $\overline{OB}$, with the same correlation value. In figure (3.4), the intrinsic velocity is the same for any space interval and its corresponding Lagrangian time interval. It is therefore constant and the Lagrangian space-time correlation function can be said to be isotropic with respect to this intrinsic velocity, or space-time isotropic. In other words, if we were to map the Lagrangian space-time correlation function in the Lagrangian frame and convert the time interval axis into a space axis using the intrinsic velocity, $\tau \rightarrow \tilde{U}\tau$, the resulting correlation function would seem isotropic.

An alternative to the constant intrinsic velocity assumption has been suggested by Lovejoy & Schertzer (1991), (1992) and Tessier et al. (1993). They have put forth the idea of a scale-dependent velocity in the context of what is called generalized scale invariance (GSI). Simply put, if we were to go from one spatial scale to another by means of a multiplicative

FIG. 3.4. An illustration of the exponential Lagrangian space−time correlation function (equation (3.8)) with an intrinsic velocity of 0.4 (arbitrary units), as seen from the Eulerian frame. The advection velocity is 0.5 (arbitrary units).

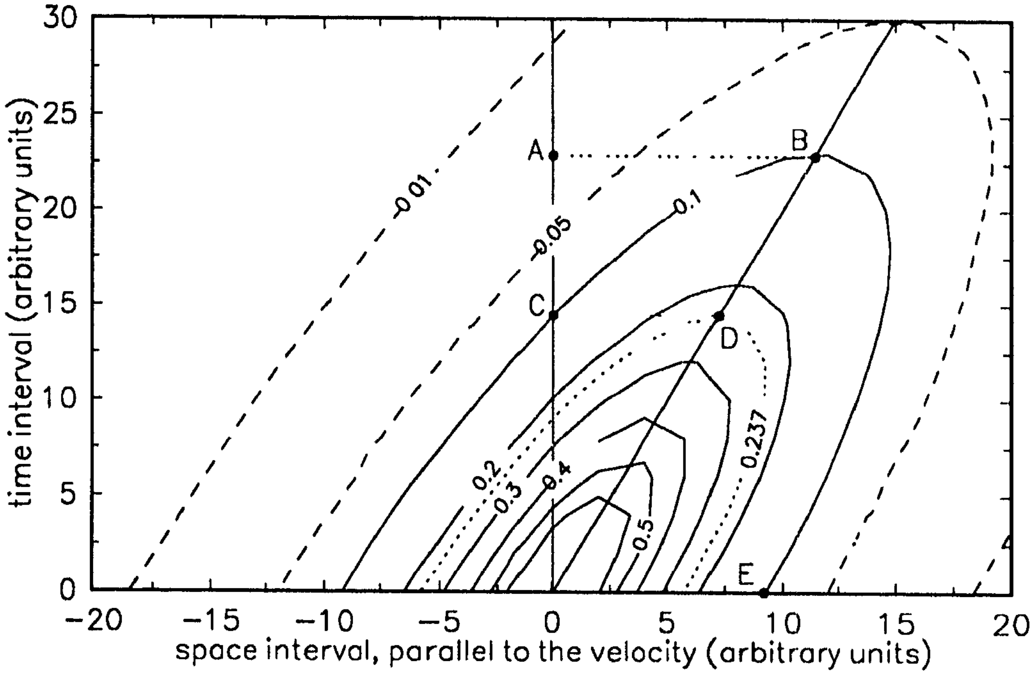

factor, $\alpha \rightarrow \alpha/\lambda$, then the corresponding correlation contour would rescale in time as, $\tau \rightarrow \tau/\lambda^{1-H}$, where $H \approx 1/3$. If we view the storm system as being forced by a turbulent velocity field with a constant mean advection velocity, then this scaling relationship deals essentially with the intrinsic velocity. As a consequence, the intrinsic velocity rescales as $\tilde{U} \rightarrow \tilde{U}\lambda^{-H}$. We can also express the intrinsic velocity as a function of the time interval, $\tilde{U} = \tilde{U}_0(\tau/\tau_0)^{\beta}$, where $\beta = H/(1-H) \approx 1/2$ and $\tilde{U}_0$ and τ_0 are some reference intrinsic velocity and time interval respectively. This kind of behavior can be seen for vertically-pointing radar data in Tessier et al. (1993), figure 22, here figure (3.5). In it, we see the contours of a two-dimensional power spectrum plotted in wavenumber - angular frequency space (k, ω) resulting from the Fourier transform of height - time reflectivity data (z,t). The contours are roughly elliptical and are elongated along the wavenumber axis close to the origin and along the frequency axis far from the origin. The change in elongation with scale is supposed to show different scaling properties for time and space. The case in question was a stratiform rain event that included a bright band.

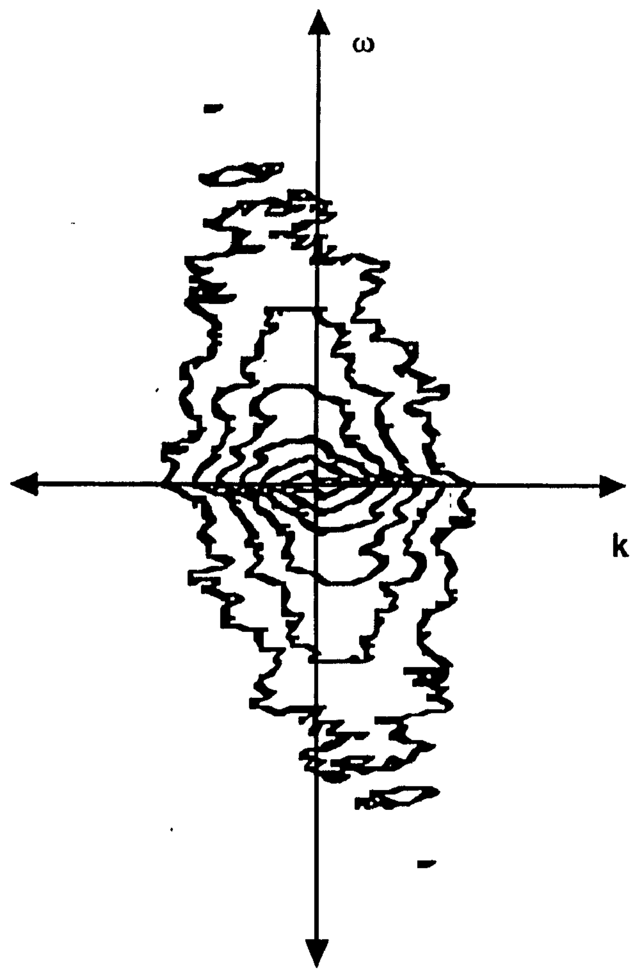

FIG. 3.5. Power spectrum contour lines in wavenumber–frequency (k, ω) space from vertically–pointing radar reflectivity data, originally in height–time (z, t) space. Note the change in elongation with distance from the origin.

It is not clear what the effect of the bright band would have on the Fourier transform. Since the bright band is narrow, long-lasting and approximately ten times brighter than its surroundings, it is possible that it would dominate at low frequencies and stretch the contours towards higher wavenumbers. Thus it produces an appearance of different scaling behaviours that would not be present in cases with no bright band or if the bright band were excluded from the analysis. Tessier et al. (1993) then show a power spectrum of the reflectivities as a function of wavenumber only, with a power-law behaviour ($E(k) \propto k^{-\beta}$) where $\beta \sim 1.4$. However the bright band was excluded and only the reflectivities under the bright band were used in the analysis. Then several reflectivity power spectra, taken over time at various fixed altitudes, were shown to have an exponent $\beta \sim 1.2$. Unfortunately, the difference between these exponents is rather small and no errors on the estimation of those exponents were given. Consequently, it is difficult to judge the significance of this difference.

Assuming that the intrinsic velocity is constant and the correlation contours are elliptical, it is possible to improve Taylor's hypothesis so as to include the intrinsic velocity in its formulation. For a given time interval $\overline{OC}$, with a Eulerian correlation of 0.1 and a Lagrangian correlation of 0.237, we wish to find the space interval $\overline{OE}$ with the same correlation as $\overline{OC}$ (see figure (3.4)). From equation (3.8) we can see that the Lagrangian space-time correlation function satisfies

$$\rho_l(0,\tau) = \rho_l(\tilde{U}\tau, 0) \tag{3.14}$$

because

$$\exp-(|\tau|/T) = \exp-(\tilde{U}|\tau|/L) \quad \text{where} \quad \tilde{U}/L = 1/T \tag{3.15}$$

which implies the space-time transformation $\alpha_l = \tilde{U}\tau$ in the Lagrangian frame. From equation (3.2.a), we see that when $\tau = 0$, $\alpha_l = \alpha_e$. Therefore, the space interval $\overline{OE}$ is equal to the time interval $\overline{OB}$ (or $\overline{OA}$) multiplied by $\tilde{U}$. We shall call the time interval $\overline{OB}$ the Lagrangian time of $\overline{OC}$ for a fixed correlation value, and shall denote it as $\tau_{l\rho}$. In terms of the Lagrangian space-time correlation function, this relationship is expressed as

$$\rho_e(0,\tau) = \rho_l(U\tau,\tau) = \rho_l(0,\tau_{l\rho}) = \rho_l(\tilde{U}\tau_{l\rho}, 0) \tag{3.16}$$

Using equation (3.8), this amounts to

$$\exp-\left(\left(\frac{U\tau}{L}\right)^2 + \left(\frac{\tau}{T}\right)^2\right)^{\frac{1}{2}} = \exp-\left(\frac{|\tau_{l\rho}|}{T}\right) = \exp-\left(\frac{\tilde{U}|\tau_{l\rho}|}{L}\right) \tag{3.17}$$

$$\frac{\tau}{T}\left[\left(\frac{U}{\tilde{U}}\right)^2+1\right]^{\frac{1}{2}}=\frac{\tau_{l\rho}}{T}=\frac{\tilde{U}\tau_{l\rho}}{L}\quad \tau,\tau_{l\rho}\geq 0 \tag{3.18}$$

and equating $\alpha_e = \tilde{U}\tau_{l\rho}$ and multiplying by L,

$$\alpha_e = \tau\left(\frac{L}{T}\right)\left(\left(\frac{U}{\tilde{U}}\right)^2+1\right)^{\frac{1}{2}} \tag{3.19}$$

Since $\tilde{U} = L/T$, we obtain the space-time relationship

$$\alpha_e = \tau\sqrt{U^2+\tilde{U}^2} \tag{3.20}$$

or

$$\rho_e(0,\tau)=\rho_e(\tau\sqrt{U^2+\tilde{U}^2},0) \tag{3.21}$$

This result applies to any Lagrangian space-time correlation function that has a constant intrinsic velocity and is isotropic with respect to that velocity. In other words, it applies to any Lagrangian space-time correlation function of the form $\rho_l(\alpha_l,\tau)=\rho_l(\tau_{l\rho})$, where $\tau_{l\rho}^2=(\alpha_l/\tilde{U})^2+\tau^2$. We shall define the function $\rho_l(\tau_{l\rho})$ as a 'radial' correlation function in analogy with a radial function in two-dimensional space, except that a velocity is needed to completely specify it. Once again, given a 'frozen' rainfall pattern, $T\to\infty$ and $\tilde{U}\to 0$, equation (3.18) becomes $\alpha_e=\tau U$ as expected. Note that for the 'frozen' rainfall pattern, the correlation contours lines in figure (3.4) would emanate from the space interval axis, on either side of the time interval axis, and would not meet on the line $\overline{OB}$. Rather, they would run parallel to that line and each other, and never meet. In that case, it is not difficult to see that the correlations along the space interval axis, in the negative direction, are projected directly onto the time interval axis with the advection velocity acting as a conversion factor. Conversely, if the advection velocity is zero but the intrinsic velocity is not, then the space-time correlations are dominated by the internal activity of the storm system and equation (3.20) becomes $\alpha_e=\tau\tilde{U}$, which reinforces the interpretation of the intrinsic velocity as defining a Lagrangian Taylor's hypothesis.

On the other hand, if the intrinsic velocity is not constant, $\tilde{U}=\tilde{U}(\tau_{l\rho})$, but the correlation contours are still elliptical, such that $\tau_{l\rho}^2=(\alpha_l/\tilde{U}(\tau_{l\rho}))^2+\tau^2$ still holds, then a radial function can no longer be defined as such. The space-time correlations can be completely specified using the Lagrangian time correlation function, the intrinsic velocity function, $\bar{U}(\tau_{l\rho})$ and the advection velocity. In that case, equation (3.21) becomes

$$\rho_e(0,\tau) = \rho_e\left(\tau\sqrt{U^2 + \bar{U}(\tau_{l\rho})^2}, 0\right) \tag{3.22}$$

where $\tau_{l\rho}$ is itself a function of τ. If we assume the scale-dependent alternative to be true, then $\tau_{l\rho}$ and τ are related by the equation, $\tau_{l\rho}^2 = (\alpha_l/\bar{U}_0)^2(\tau_0/\tau_{l\rho}) + \tau^2$, and it is not difficult to see that the space-time transformation for Taylor's hypothesis becomes non-linear.

4. Spatial averaging and space-time correlations

All instruments have limits to their resolution, temporal as well as spatial. Radar is no exception, especially with regard to spatial resolution. Also, the temporal characteristics of rainfall depend a great deal on the spatial resolution of measurement. For instance, Bell (1987) observed, using data collected by Laughlin (1981), that the decorrelation time τ_A for rainfall averaged over an area $A = L^2$ varies as $\tau_A = cL^{2/3}$, where c is some constant. This is important because it affects issues such as predictability or the proper temporal resolution for describing events at a given scale. It may also give insight into the dynamics of rainfall.

In this paper, we shall treat spatial resolution as the independent variable and the corresponding space-time correlation structure as a function of the former. Therefore we shall not attempt to alter the temporal resolution of the data. In fact, we shall assume that the data consists of instantaneous snapshots five minutes apart. This is not strictly true of course, as the radar maps are actually composites of smaller picture elements taken at different times over a span of five minutes. But in the Eulerian frame, the time between an element on one map and the corresponding element on the succeeding map is five minutes. We choose to neglect the changes that occur to this rule when we move to the Lagrangian frame.

Given a random space-time rainfall field $R(x,y,t)$, we obtain a spatially averaged field.

$$R_A(x,y,t) = \frac{1}{D^2}\int_{x-D/2}^{x+D/2}\int_{y-D/2}^{y+D/2} R(x',y',t)dy'dx' \tag{4.1}$$

where $A = D^2$ and D shall be known as the averaging length. The averaging is done relative to a 'top hat' weighting function. That is, the averaging gives equal weight to the field within the square A and ignores the field outside this square. An alternative would be the Gaussian weighting function (Zawadzki, 1973b) which imitates the averaging effect of a radar beam. The covariance of the averaged field, assuming it exists for the original field, is then

$$\mathrm{Cov}_A(x_1,y_1,t_1,x_2,y_2,t_2) = \mathrm{E}[R'_A(x_1,y_1,t_1)R'_A(x_2,y_2,t_2)] \tag{4.2}$$

where E[ ] denotes an ensemble average and $R'_A(x,y,t) = R_A(x,y,t) - \overline{R_A(x,y,t)}$, where $\overline{R_A(x,y,t)}$ is the ensemble average of the spatially averaged field, which, incidentally, is the same as the spatial average of the ensemble average of the original field. Using stationarity and homogeneity and performing the spatial averaging integrals last, equation (4.2) becomes

$$\mathrm{Cov}_A(\alpha,\beta,\tau)=\frac{1}{D^4}\int_{x_1-D/2}^{x_1+D/2}\int_{y_1-D/2}^{y_1+D/2}\int_{x_2-D/2}^{x_2+D/2}\int_{y_2-D/2}^{y_2+D/2}\mathrm{Cov}(\alpha',\beta',\tau)dy_2'dx_2'dy_1'dx_1' \tag{4.3}$$

where $\alpha=x_2-x_1$, $\beta=y_2-y_1$ and $\tau=t_2-t_1$

Since the covariance depends only on intervals, we can set $x_1=0$, $y_1=0$ and consequently $\alpha=x_2$, $\beta=y_2$. We can simplify this further by setting $\beta=0$, there is no loss of generality if the field is isotropic. We now have,

$$\mathrm{Cov}_A(\alpha,0,\tau)=\frac{1}{D^4}\int_{-D/2}^{D/2}\int_{-D/2}^{D/2}\int_{\alpha-D/2}^{\alpha+D/2}\int_{-D/2}^{D/2}\mathrm{Cov}(\alpha',\beta',\tau)dy'_2dx'_2dy'_1dx'_1 \tag{4.4}$$

One can clarify this even more by changing the variables of integration. That is, we integrate with respect to $\alpha'=x'_2-x'_1$, $\eta'=x'_2+x'_1$, $\beta'=y'_2-y'_1$ and $\lambda'=y'_2+y'_1$. We obtain, after some calculation,

$$\mathrm{Cov}_A(\alpha,0,\tau)=\frac{2}{D^4}\int_0^D(D-\beta')\left\{\int_{\alpha-D}^{\alpha+D}D\,\mathrm{Cov}(\alpha',\beta',\tau)d\alpha'\right.$$
$$\left.+\int_{\alpha}^{\alpha+D}(\alpha-\alpha')\mathrm{Cov}(\alpha',\beta',\tau)d\alpha'-\int_{\alpha-D}^{\alpha}(\alpha-\alpha')\mathrm{Cov}(\alpha',\beta',\tau)d\alpha'\right\}d\beta' \tag{4.5}$$

Note that a derivation very similar to the preceding may be found in Vanmarcke (1983). Also, the derivation of this result made use of the quadrant symmetry of the covariance function. Therefore, the function in question is the Lagrangian covariance function. Setting $\alpha=0$ and using quadrant symmetry again, we obtain

$$\mathrm{Cov}_A(0,0,\tau)=\frac{4}{D^4}\int_0^D\int_0^D(D-\alpha')(D-\beta')\mathrm{Cov}(\alpha',\beta',\tau)d\beta'd\alpha' \tag{4.6}$$

which is in fact the variance of the spatially averaged field when $\tau=0$. We are now in a position to find the space-time correlation function of the spatially averaged field since,

$$\rho_A(\alpha,0,\tau)=\frac{\mathrm{Cov}_A(\alpha,0,\tau)}{\mathrm{Cov}_A(0,0,0)} \tag{4.7}$$

Given that $\mathrm{Cov}(\alpha,0,\tau)=\sigma^2\rho(\alpha,0,\tau)$, where σ^2 is the constant variance of the field, we can find $\rho_A(\alpha,0,\tau)$ in terms of $\rho(\alpha,0,\tau)$ only.

$$\rho_A(\alpha,0,\tau)=\frac{1}{2\int_0^D\int_0^D(D-\alpha')(D-\beta')\rho(\alpha',\beta',0)d\beta'd\alpha'}\left\{\int_0^D(D-\beta')\left[\int_{\alpha-D}^{\alpha+D}D\rho(\alpha',\beta',\tau)d\alpha'\right.\right.$$

$$\left.\left.+\int_{\alpha}^{\alpha+D}(\alpha-\alpha')\rho(\alpha',\beta',\tau)d\alpha'-\int_{\alpha-D}^{\alpha}(\alpha-\alpha')\rho(\alpha',\beta',\tau)d\alpha'\right]d\beta'\right\} \tag{4.8}$$

Again, it is the Lagrangian space-time correlation function we are dealing with. Equation (4.8) can be made simpler if we consider only the temporal behaviour of the spatially averaged correlation function, that is $\alpha = 0$.

$$\rho_A(0,0,\tau)=\frac{1}{2\int_0^D\int_0^D(D-\alpha')(D-\beta')\rho(\alpha',\beta',0)d\alpha'd\beta'}\left\{\int_0^D(D-\beta')\left[\int_{-D}^{D}D\rho(\alpha',\beta',\tau)d\alpha'\right.\right.$$

$$\left.\left.+\int_0^D(-\alpha')\rho(\alpha',\beta',\tau)d\alpha'-\int_{-D}^{0}(-\alpha')\rho(\alpha',\beta',\tau)d\alpha'\right]d\beta'\right\} \tag{4.9}$$

Given quadrant symmetry, $\rho(\alpha,\beta,\tau)$ is an even function. Therefore the bounds of the first integral of the numerator can go from 0 to D and the integral is multiplied by 2, the third integral can be transformed into the second integral. The same process was done to the denominator and the result is

$$\rho_A(0,0,\tau)=\frac{\int_0^D\int_0^D(D-\alpha')(D-\beta')\rho(\alpha',\beta',\tau)d\alpha'd\beta'}{\int_0^D\int_0^D(D-\alpha')(D-\beta')\rho(\alpha',\beta',0)d\alpha'd\beta'} \tag{4.10}$$

Immediately, we see that if the temporal part of the correlation were separable from the spatial part, that is $\rho(\alpha,\beta,\tau)=\rho_s(\alpha,\beta)\rho_t(\tau)$ as it is sometimes assumed (Rodriguez-Iturbe & Mejia, 1974a,b), the temporal part could be factored out of the integrals, leaving $\rho_A(0,0,\tau)=\rho_t(\tau)$, for any A. This means that spatial averaging has no effect on the temporal aspect of a separable correlation function, which is in contradiction to the result observed by Bell (1987).

It would be interesting to see the effect of spatial averaging on the simple exponential space-time correlation function introduced in equation (3.8). In order to apply equation (4.8), we must expand the correlation function into the form

Simulated space correlation

FIG. 4.1. The effect of spatial averaging on the spatial component of the space–time exponential correlation function, eq.(4.11). D is the length of one side of the square averaging area.

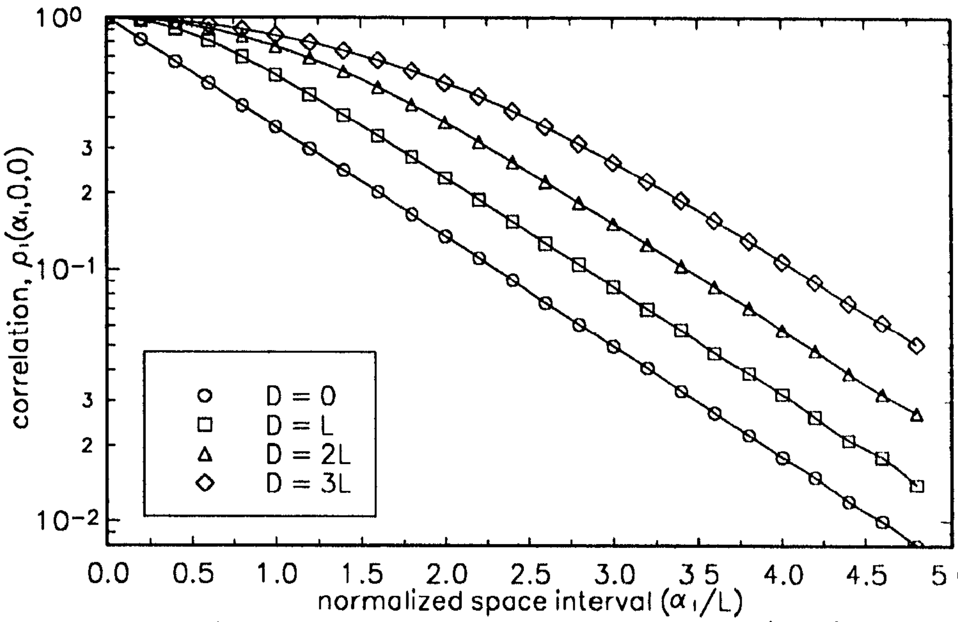

L is the characteristic length from equation (4.11)

$$\rho_l(\alpha_l, \beta_l, \tau) = \exp - \left(\left(\frac{\alpha_l}{L}\right)^2 + \left(\frac{\beta_l}{L}\right)^2 + \left(\frac{\tau}{T}\right)^2 \right)^{\frac{1}{2}} \qquad (4.11)$$

where isotropy is assumed. Clearly, this function is difficult to evaluate analytically in equation (4.8). Therefore, numerical methods are used to evaluate the integrals. The resulting correlation functions for various values of D along the lines $\beta_l = 0$, $\tau = 0$ and $\alpha_l = 0$, $\beta_l = 0$ are shown in figures (4.1) and (4.2), respectively.

These figures show that upon spatial averaging, an initially exponential correlation function is no longer a pure exponential. This is understandable for the spatial component, because if we have two non-zero averaging areas (such that $D > 0$), where one is superimposed on top of the other, and we move one area by an infinitesimally small distance, the correlation between them should be arbitrarily close to one. Therefore, the derivative of the correlation function with respect to α_l must be zero at $\alpha_l = 0$, which explains the shape of the curves at small intervals in figure (4.1).

Simulated time correlation

FIG. 4.2. The effect of spatial averaging on the temporal component of the space–time exponential correlation function, eq.(4.11). D is the length of one side of the square averaging area.

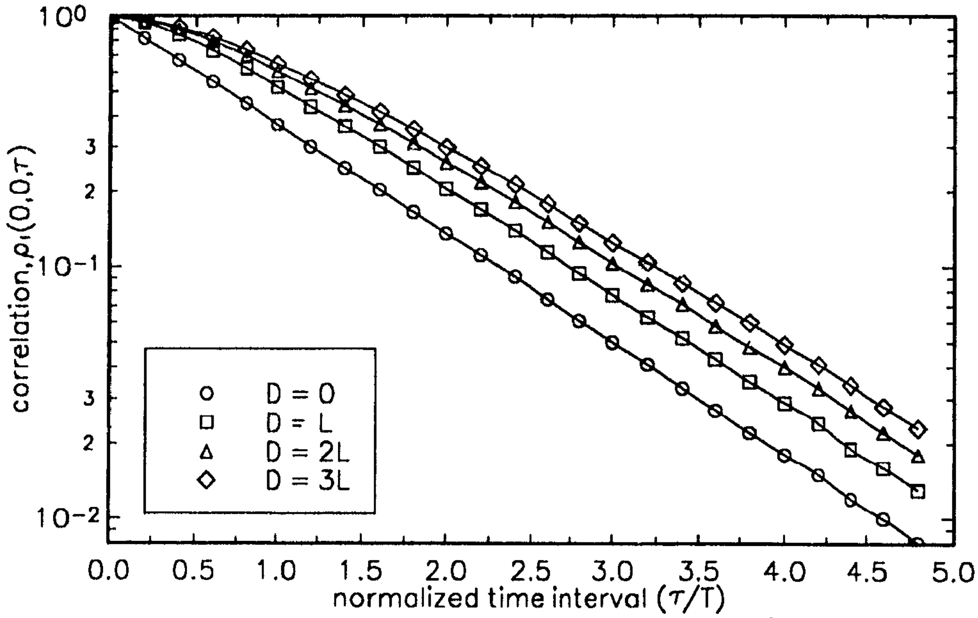

T is the characteristic time from equation (4.11)

Of greater interest is shape of the curves at large intervals. In figures (4.1) and (4.2), we see that the curves of the spatially averaged correlation functions are very nearly parallel to the original exponential line. In other words, for large intervals, the spatially averaged correlation function differs from the exponential only by a multiplicative constant which is a function of the averaging length, D. There is reason to believe this to be the case when one considers the one-dimensional correlation function, $\rho(\alpha) = \exp - |\alpha/L|$, and the one-dimensional form of equation (4.8).

$$\rho_D(\alpha) = \frac{1}{2\int_0^D (D-\alpha')\rho(\alpha')d\alpha'} \left\{ \int_{\alpha-D}^{\alpha+D} D\rho(\alpha')d\alpha' + \int_{\alpha}^{\alpha+D} (\alpha-\alpha')\rho(\alpha')d\alpha' - \int_{\alpha-D}^{\alpha} (\alpha-\alpha')\rho(\alpha')d\alpha' \right\} \quad (4.12)$$

Placing the one-dimensional correlation function in this formula and assuming that $\alpha \geq D$, one obtains;

$$\rho_D(\alpha) = \left\{ \frac{\cosh(D/L) - 1}{\exp(D/L) + (D/L) - 1} \right\} \exp -|\alpha/L| \tag{4.13}$$

which is the original correlation function multiplied by a function of D. It is then reasonable to assume that the same separability applies, either exactly or approximately, to the spatial and temporal components of the space-time exponential correlation function. However, it is also clear from figures (4.1) and (4.2) that the temporal component is multiplied by an averaging function, $M_\tau(D)$, which is different than the spatial averaging function, $M_\alpha(D)$. Mathematically, we have $\rho_{lA}(0,0,\tau) = M_\tau(D)\rho_l(0,0,\tau)$ and $\rho_{lA}(\alpha_l,0,0) = M_\alpha(D)\rho_l(\alpha_l,0,0)$, where $M_\tau(D) \neq M_\alpha(D)$. This is because the intervals between the lines in figure (4.1) are different than the intervals in figure (4.2). This means that the initial space-time isotropy is lost under spatial averaging, which is to be expected since the space and time components of the correlation function are not transformed in the same way.

Simulated intrinsic velocity functions

FIG. 4.3. The intrinsic velocities as a function of the normalized time interval for various averaging lengths (D) from the exponential Lagrangian space–time correlation function with characteristic length L and time T.

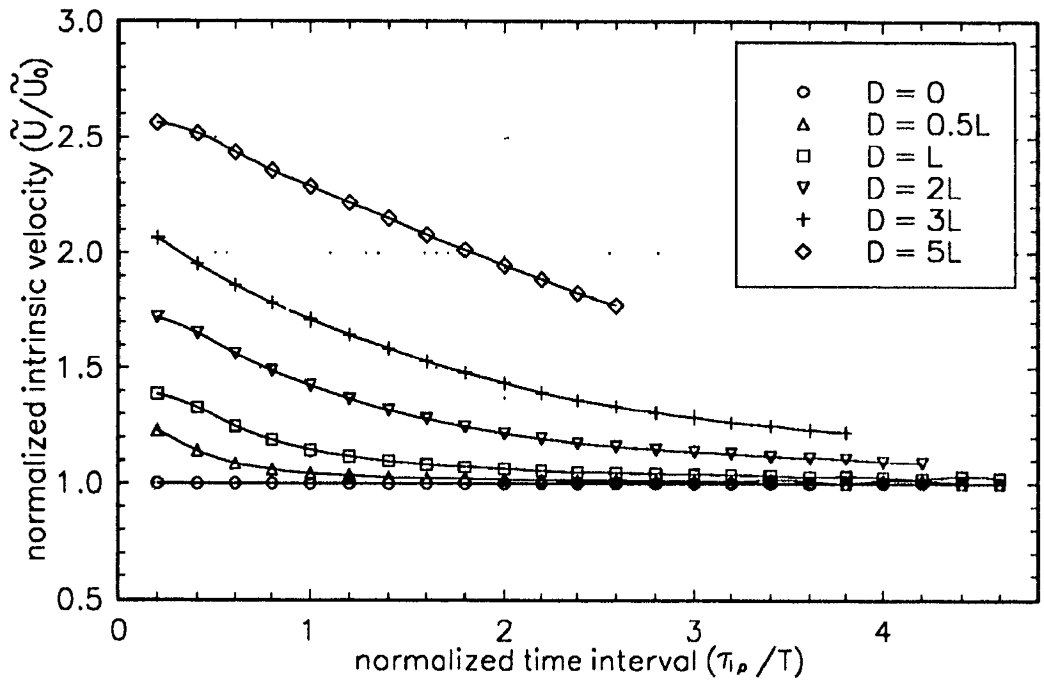

The effect of spatial averaging on the intrinsic velocities is shown in figure (4.3). There we see the function $\tilde{U}(\tau_{l\rho})$ obtained by simply finding the correlation at the point $(0,0,\tau)$, then finding the corresponding point $(\alpha_l,0,0)$ and then taking the ratio α_l/τ. Figure (4.3) demonstrates that the intrinsic velocity increases with increasing averaging length for short time intervals, and decreases with increasing time intervals such that it asymptotically approaches the original intrinsic velocity. Meaning that equation (3.21) would hold approximately only for long time intervals given spatial averaging and an exponential Lagrangian space-time correlation function (equation (4.11)). This result implies that spatial averaging introduces a scale, namely D, near which spatial correlations are strong and do not change very rapidly with decreasing space interval, especially when compared with the change with decreasing time interval. Therefore, the correlation contours will become more and more elongated along the space interval axis as we get closer to the origin of the space-time correlation map. Physically, this means that spatial averaging introduces a minimum length scale for the features of the random field but not necessarily a minimum time scale for those features.

5. Data analysis

The data used in this study consists of radar reflectivity CAPPI (Constant Altitude Plan Position Indicator) maps transformed to represent rainfall. Reflectivity to rainfall relationships (Z-R relationships) have the general form

$$Z = aR^b \tag{5.0.1}$$

where Z is the radar reflectivity, R is the rain rate in millimeters per hour and a and b are constants. There is much debate about what the value of a and b should be, but we use $a = 200$ and $b = 1.6$. The CAPPIs were obtained with the McGill FPS-18 weather radar, the characteristics of which can be found in Table (5.0.1). For each rain event three sequences of CAPPIs are used, one with a resolution of 2 km and a diameter of 480 km, another with a resolution of 1 km, diameter of 240 km and another with 250 m resolution with a 96 km diameter.

Rain events were recorded for most of 1992 and were selected according to two criteria; length of time of the recorded sequence and apparent statistical properties. The first criterion deals mainly with the 250 m resolution CAPPIs since special equipment must be installed to record them. Furthermore, only approximately four hours may be stored with this equipment. Consequently, some interesting rain events were discarded because the equipment was activated too early or too late. The second criterion deals with the appearance of the rain events. Often, rain would be caused by fronts which would appear as a line of highly convective rainfall followed by stratiform rain. Such rain events are manifestly inhomogeneous since they are composites of different precipitation processes. And since the theory developed in the previous sections assume homogeneity and stationary, we can only select those cases with no ostensive inhomogeneity or nonstationarity. Of all the cases recorded, therefore, two rain events are chosen, the first occurred on the 19th of June, 1992, the second on the 31st of July, 1992. Illustrations of sample CAPPIs for the two cases can be seen in figures (5.0.1) and (5.0.2). Note that the figures show the rain events in decibels of reflectivity (dBZ) while the correlations are computed using rain rates.

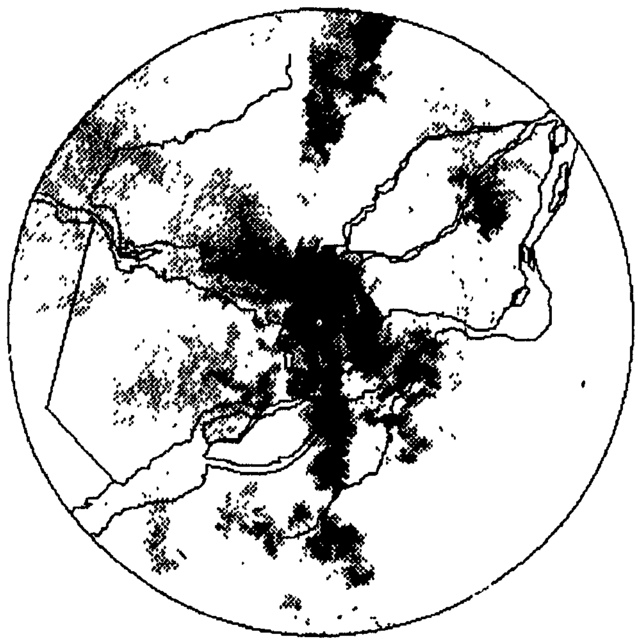

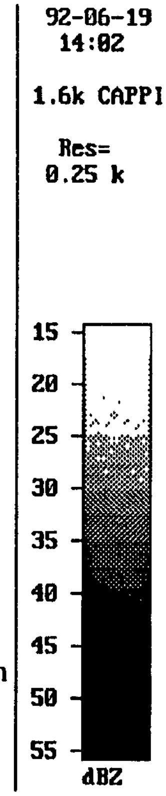

FIG. 5.0.1. Radar reflectivity CAPPI from a convective rain case on the 19th of June, 1992, is viewed at an altitude of 1.6 km and a resolution of 250 m. The storm system moved with a speed of approximately 40 km/hr towards the north-east.

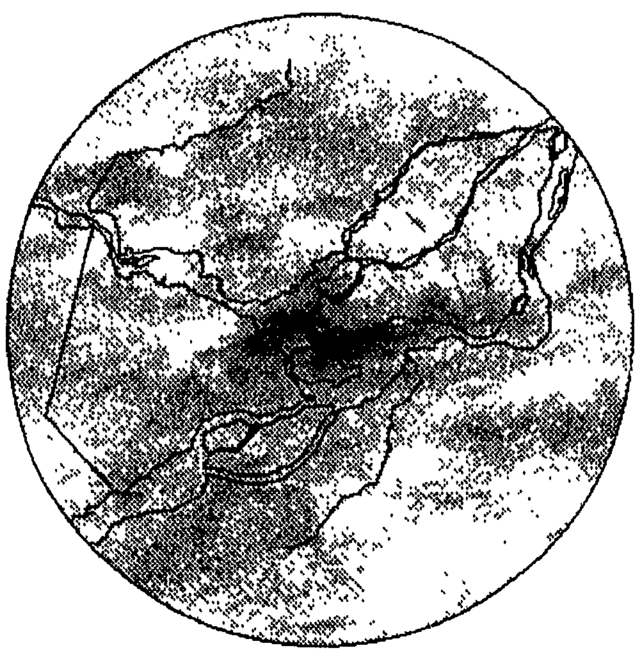

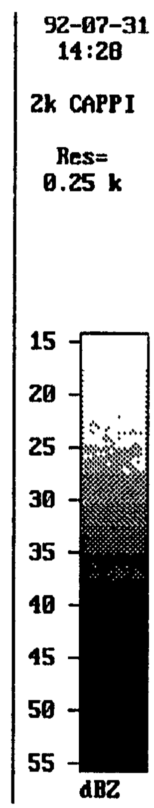

FIG. 5.0.2. Radar reflectivity CAPPI from a stratiform rain case on the 31st of July, 1992, is viewed at an altitude of 2.0 km and a resolution of 250 m. The storm system moved with a speed of approximately 50 km/hr towards the north-east.

Table 5.0.1. McGill Radar characteristics

Wavelength [cm]	10.4
Peak power [kW]	1000
Beam width [deg]	0.86
Pulse length [μs]	1
Minimum detectable reflectivity at 200 km [dBZ]	18
Range of elevation angles [deg]	0.5 - 34.4

19 June 1992

On the 19th of June, 1992, a low pressure trough beginning over Lake Ontario and extending in a north-east direction parallel to the St-Lawrence valley caused south-westerly winds over the Montreal region, bringing warm and moist air in the region. Since the environment was particularly unstable, a mesoscale convective system (MCS) formed and moved over the radar site from late in the morning until late in the afternoon. An atmospheric sounding carried-out in Maniwaki, approximately 200 km north-west from the radar site, revealed a convective energy of 1625 J/Kg. The lack of a front makes this case well suited for study since it contains no obvious structure and can be approximated as statistically homogeneous. The data collected begins at 12:15 and ends at 16:20 local time. The 1 and 2 km resolution CAPPIs have an altitude of 3 km and the 250 m resolution CAPPIs have an altitude of 1.6 km.

31 July 1992

On the 31st of July, 1992, a low pressure system centered over Pennsylvania advected warm air into the Montreal region. The air was mildly unstable and had a convective energy of 115 J/Kg. The stratiform precipitation it produced was widespread with only a few weak cells. It therefore had a more or less uniform appearance. The precipitation lasted from late morning until late afternoon. Data was collected starting from 13:20 until 17:10. All CAPPI sequences have an altitude of 2 km.

Data processing for the CAPPIs

The radar emits 300 pulses every second (it has a pulse repetition frequency, PRF, of 300 Hz). And given the rotation rate of the radar (1 rotation every 10 seconds) this leaves approximately 8 pulses for each 1° wide radial scan. From these pulses the mean value of the reflectivity, which is related to the liquid water content of the scanning volume, is retrieved from the fluctuations caused by the interference of the radio waves with the droplets. The method for the 1 or 2 km resolution CAPPIs consists of collecting only one pulse for each 1° radial scan (thus ignoring the seven others) and finding the maximum reflectivity value in each 1 km wide range bin. The maximum reflectivity is then transformed into the mean value by an empirical relationship, (Marshall 1971) and the mean is transformed into a rainfall estimate. The rainfall values are still in spherical coordinates, so they are averaged in such a way as to yield CAPPIs in Cartesian coordinates. The number of values averaged for a given pixel decreases with the distance from the center of the CAPPI.

The method for the 250 m resolution CAPPIs, on the other hand, employs every pulse. For each 75 m range bin of every pulse, the logarithm of the reflectivity is stored and then mapped into a 250 m resolution CAPPI. Each pixel of the CAPPI contains the average of the logarithms of the reflectivity which is then transformed into the logarithm of the average reflectivity according to certain theoretical assumptions (Marshall and Hitschfeld 1953, Wallace 1953). Finally, the logarithm of the average reflectivity is exponentiated and transformed into rainfall using the equation (5.0.1).

5.1. Defining a scale

Although the CAPPIs consist of square maps subdivided into smaller square picture elements (henceforth called pixels) of a given resolution, the task of defining a scale is not that straightforward. The radar beam has a finite angular width, so it gets wider as the range increases. Therefore around the edges of the CAPPI the width of the beam can be greater than the size of a pixel. This would introduce a dependance between neighboring pixels and affect the statistics. Consequently, we shall only collect statistics within the range where overlapping does not occur. To determine at what range the overlapping of the beam begins, we start by noting that the beamwidth is at most one degree. So we can find the spatial beamwidth using the formula,

$$\Delta x = r \sin[(\pi/180)\Delta\theta] \qquad (5.1.1)$$

where r is the range in kilometers, $\Delta\theta$ is the angular beamwidth in degrees and Δx is the spatial width of the beam at that range, also in kilometers. Therefore, if we set the spatial resolution equal to Δx, we have a maximum range beyond which overlapping occurs for that resolution. We can determine the maximum range in terms of pixels by dividing it by the resolution. From equation (5.1.1) we get

$$\frac{r_{\max}}{\Delta x} = \operatorname{cosec}\left[\left(\frac{\pi}{180}\right)\Delta\theta\right] \tag{5.1.2}$$

where $\Delta\theta \approx 1°$ and so the maximum range is 57.3 pixels long which we approximate to 60. This means that as the resolution decreases the maximum range increases such that we have the same number of pixels. A limit is reached when the maximum range is greater than the size of the CAPPI and so the number of pixels decreases with increasing $r_{\max}$. It is important to distinguish between the pixels given in the original data and the pixels obtained after averaging the data. The larger pixel is the average of the smaller, original pixels. In this way, the resolution is degraded, which allows for greater range and for greater available area in such a manner that the number of pixels remains constant. Note that the resolution used in this analysis shall range from 500 m to 8 km. The 250 m resolution analysis shall be excluded because we only have a 30 km diameter area available. Given an advection velocity of approximately 40 km/hr, this only leaves a 45 min time interval when a given rainfall pattern is in view.

Now that we have a method describing how to use the most data for a given resolution, we must consider what are its possible effects on the statistics. If there is a storm system with a size comparable to the size of the largest CAPPI, a constant advection velocity and a homogeneous interaction with the ground, then the statistics taken over the entire duration of the sequence are identical for a region of any size and location. This is because the storm passes over every point for approximately the same length of time. On the other hand, if there are noticeable interactions at specific places such as orographic effects or strong and localized heat and moisture fluxes from the ground, then the statistics are not homogeneous. There are also range dependent effects due to the curvature of the earth and in the processing of the reflectivity data. Although the data analysis assumes homogeneity and stationarity, we must bear these facts in mind when interpreting the results.

5.2. Defining a space-time correlation function

In chapter 2.1, we defined the covariance function for a stationary and homogeneous random field as

$$\mathrm{Cov}(\alpha,\beta,\tau) = \mathrm{E}[(R(x+\alpha, y+\beta, t+\tau) - \overline{R})(R(x,y,t) - \overline{R})] \tag{5.2.1}$$

where $\overline{R}$ is the ensemble mean which is constant over time and space. In practice, the only way we can approximate averages over the ensemble is to average over the space-time domain of a single realization of an ergodic random field. Thus, for a sequence of rainfall maps, we use

$$< R > = \frac{1}{AT} \sum_{i,j,k} R(x_i, y_j, t_k) \tag{5.2.2}$$

where A is the available area for that particular resolution, T is the duration of the sequence and $<\ >$ denotes an average over AT. We have a summation rather than an integral because the rainfall maps are composed of discrete pixels. Similarly, A and T are in fact dimensionless integers since they refer to the number of pixels in a map and the number of maps respectively. The covariance function is given by

$$\mathrm{Cov}(\alpha, \beta, \tau) = \frac{1}{A'T'} \sum_{i',j',k'} [R(x_{i'} + \alpha, y_{j'} + \beta, t_{k'} + \tau) - < R >] \times [R(x_{i'}, y_{j'}, t_{k'}) - < R >] \tag{5.2.3}$$

where A' is the area within A that contains all starting points for the displacement vector such that the end points are also contained in A. In other words, let us suppose that $\tau = 0$ and we have a spatial displacement $\overrightarrow{\Delta x} = (\alpha, \beta)$ for a given map, the area A' is the intersection between two copies of that map with a relative displacement $\overrightarrow{\Delta x}$. So if the available area is a circle, A' has the shape of a football. The same reasoning applies for T' except that we have the simple expression $T' = T - \tau$ because there is only one dimension to contend with. Of course, as in sections 2.1 and 4, the correlation function is

$$\rho(\alpha, \beta, \tau) = \mathrm{Cov}(\alpha, \beta, \tau)/\mathrm{Cov}(0,0,0) \tag{5.2.4}$$

The expression for the covariance contains $< R >$ which was obtained by averaging over A and T, not A' and T'. This means that

$$< [R(x,y,t) - < R >] >' = \frac{1}{A'T'} \sum_{i',j',k'} [R(x_{i'}, y_{j'}, t_{k'}) - < R >] \tag{5.2.5}$$

may not equal zero. Note that $<\ >'$ implies an average over $A'T'$. Indeed, as the displacement tends towards the size of A ($|\overrightarrow{\Delta x}| \to A^{\frac{1}{2}}$) and $\tau \to T$, the region of averaging tends to the same size or smaller than the correlation length and time, so that all the pixels in it are strongly correlated with each other. Therefore, the covariance at such a displacement becomes very unreliable. Another technique would be to define the mean rain rate as the average over A' and T', therefore $< R >$ changes with the displacement such that equation (5.2.5) equals zero by definition. But at large displacement, $< R >$ becomes highly variable and therefore a random variable itself rather than a meaningful characterization of the random field. Again, there is no reason to believe this method would improve the covariance at large displacements. So we choose to define $< R >$ over the entire space-time region once and for all.

One fact to consider is that the sequences last for approximately four hours and the time interval of the correlation function never exceeds two hours. Since the maps are five minutes apart, this means that there are approximately 24 pairs of maps two hours apart. If the correlation time is of the order of thirty minutes, which is a reasonable estimate, this gives us the equivalent of four independent observations in time. Assuming the probability density of rain rate at a point is lognormal and that the mean and the standard deviation are related by $<R^2>= 4.35 <R>^2$ and consequently, $\sigma = 1.83 <R>$, as was shown by Zawadzki (1973a) for one storm system, we can estimate the error on the mean for a given number of independent observations;

$$E = z_{\alpha/2}\left(\frac{\sigma}{\sqrt{n}}\right) \qquad (5.2.6)$$

where E is the maximum error of the estimate of the mean for a normal population, $z_{\alpha/2}$ is the deviation from the mean for a standard normal distribution with a confidence interval of α. If the spatial displacement is so large that each map holds only one equivalent independent observation in space, and the required confidence level is 90%, this yields $z_{\alpha/2} = 1.65$, $n = 4$ and finally, $E \approx 1.5 <R>$. This crude approximation demonstrates that for large space-time displacements, the error on an estimation of the mean is of the same order as the mean and that there is a minimum of four independent observations. The same can probably be said for the estimation of the covariance at large displacements. This is important because an unreliable estimation of the covariance also means an unreliable estimation of the correlation. And since Taylor's hypothesis depends on comparing the correlation over space with that over time, an unreliable correlation function for large displacements, in space and time, would jeopardize any attempt to evaluate it's validity. For example, if Taylor's hypothesis was in fact valid for a very long time, the correlation functions might fortuitously diverge and give an unreliable estimate of the cut-off time.

An alternative to equation (5.2.3) exists in the work of Zawadzki (1972, 1973a and 1975), Drufuca & Zawadzki (1975) and Lachapelle (1990), among others. Namely, the mean is not subtracted from the rain field,

$$C(\alpha,\beta,\tau) = \frac{<R(x+\alpha, y+\beta, t+\tau)R(x,y,t)>'}{<R^2>} \qquad (5.2.7)$$

where $C(\alpha, \beta, \tau)$ is the function introduced in section 3. This function is ideal for treating isolated storm systems. Given a storm that can be easily identified and is completely contained in an area A_s and in a time interval T_s, that is over its lifetime T_s it never crosses the boundary of A_s, then the statistic

$$< R(x+\alpha, y+\beta, t+\tau) R(x, y, t) >' = \frac{1}{A'T'} \sum_{i',j',k'} R(x_{i'}+\alpha, y_{j'}+\beta, t_{k'}+\tau) R(x_{i'}, y_{j'}, t_{k'}) \tag{5.2.8}$$

where $A_s \subset A'$ and $T_s \subset T'$, varies as $(A'T')^{-1}$ with increasing A' and T'. And since this also applies when $\alpha = \beta = \tau = 0$, the function $C(\alpha, \beta, \tau)$ remains invariant with respect to A' and T' as long as they completely contain the storm. In this way, the manifestly inhomogeneous and non-stationary situation of a storm in one region and time interval and nothing anywhere else, can be treated in a manner analogous to a homogeneous and stationary random field. This method only works when the entire space-time extent of an isolated storm system is available for analysis and that the analysis focuses exclusively on that storm system. However, in this work we are concerned with storm systems that are bigger than the region of observation with rainfall structures that flow in and out of that region. In our analysis the spacing between isolated showers is considered as much a part of the rain field as the showers themselves. In any case, it is not always possible to isolate individual elements from the rest of the rain field. This is certainly true for the stratiform case (see figure (5.0.2)). Under these conditions, the original invariance is lost because as we increase the area of averaging, new rainfall may be included which can change the value of the function. Furthermore, since the mean used in equation (5.2.3) is a constant (i.e. not dependent upon A' or T') the square brackets product in equation (5.2.3) can be expanded as a polynomial and an approximate linear relationship between $\rho(\alpha, \beta, \tau)$ and $C(\alpha, \beta, \tau)$ can be established (see appendix B).

$$C(\alpha, \beta, \tau) = \left(\frac{\sigma^2}{< R^2 >} \right) \rho(\alpha, \beta, \tau) + \frac{< R >^2}{< R^2 >} \tag{5.2.9}$$

When there is perfect correlation, $\rho(0,0,0) = 1$ and $C(0,0,0) = 1$, but when two points are uncorrelated, $\rho(\infty, \infty, \infty) = 0$ which implies $C(\infty, \infty, \infty) = < R >^2 / < R^2 >$. Therefore, when using the C-correlation function, we do not know how close we are to complete decorrelation without knowledge of the mean. And if we allow knowledge of the mean, then we might as well use the ρ-correlation function. In any event, the choice of correlation function is irrelevant as far as the intrinsic and advection velocities are concerned. Those velocities depend on the geometry of the correlation contours and not on the value of the correlation along those contours. And since the transformation from one function to the other is linear, it will not alter the shape of the contours.

5.3. Defining a velocity

Of equal importance to the definition of a scale is the definition of a velocity. It is the velocity which determines the space to time relationship essential for Taylor's hypothesis. The apparent motion of a storm system depends not only on the large scale forcing driving it, but also on the internal developments of the system. A multicell thunderstorm, for example, has cells which move in one direction, but the generation and dissipation of cells is such that the storm as a whole appears to be moving at an angle to that direction. In the cases studied here, we have verified that the cells, or rather the small, high intensity features of the system, move with approximately the same velocity as the broad, low intensity regions.

FIG. 5.3.1. The time-averaged advection velocities of the areas of rain exceeding the threshold for the rain event on the 19th of June, 1992, and on the 31st of July, 1992, using the 1 km resolution CAPPIs with no spatial averaging.

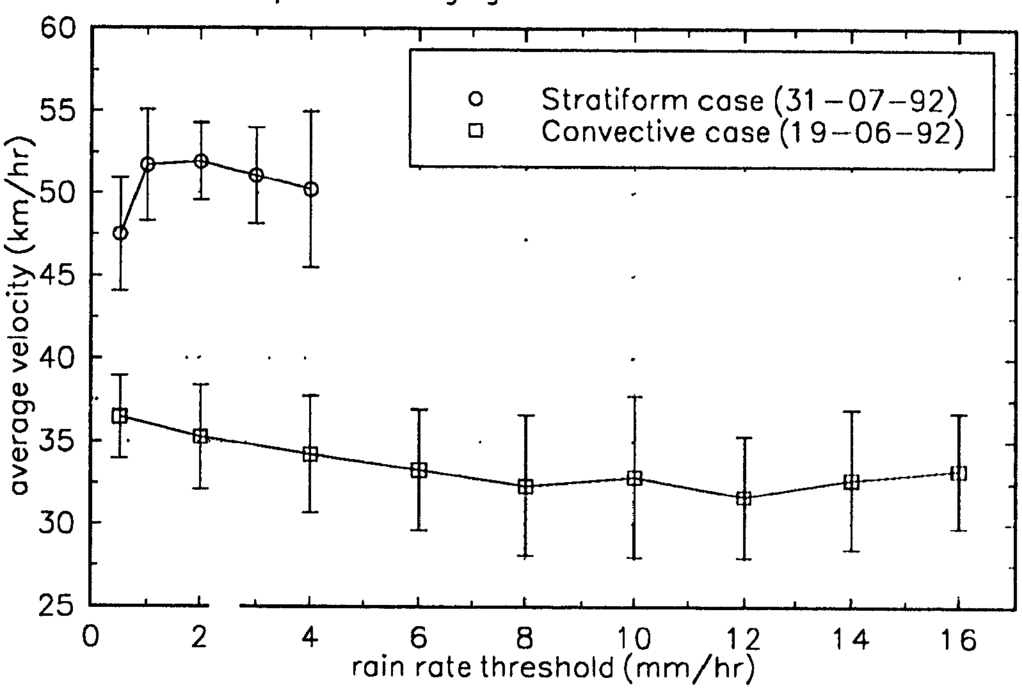

This is shown in figure (5.3.1) where we see the time-averaged velocity of the precipitating regions with a rain rate greater than or equal to the thresholds indicated. The internal structure of those regions was ignored when determining the velocities. Only the displacements from one CAPPI to the next of the outlines of the exceeding regions ascertain the velocities. The figure shows a slight decreasing trend of the velocity with increasing threshold value for the convective case. Even with this trend, the average velocity never deviates more than 16% from its initial value at 0.5 mm/hr. The stratiform case has no obvious trend with the threshold value and the average velocity never deviates more than 10% from the value at 0.5 mm/hr. Note that the error bars represent the standard deviations from the average and that the maximum threshold represents the level past which the exceeding regions are too small and sparse to give a reasonable estimate of the velocity.

Eulerian space–time correlation

FIG. 5.3.2. The space–time correlations in the Eulerian frame for the rain event on the 19th of June, 1992. Notice a distinct slant due to the overall velocity. The resolution is 500 m.

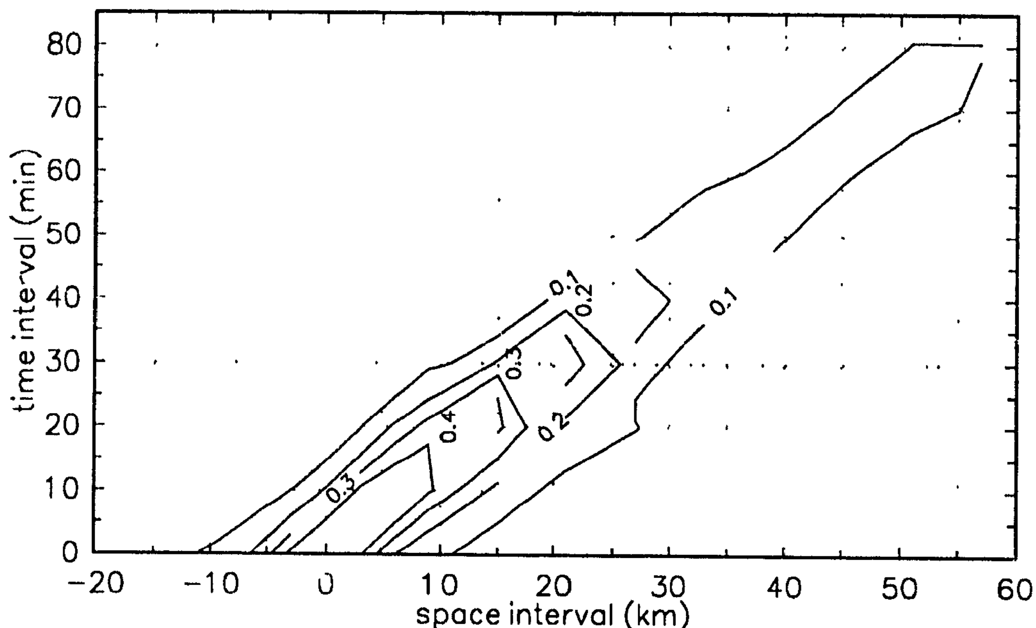

The space interval vector has the same orientation as the velocity.

The definition of the advection velocity in this work is the slope of the line which starts at the origin of the Eulerian space-time correlation map and extends along the direction which minimizes the rate of decorrelation on the line. For example, figure (5.3.2) shows just such an

Eulerian space-time correlation map, and the velocity is clearly the line which extends along the band of high correlation. This has a value of about 38.5 km/hr and once we perform a coordinate transformation as described by equations (3.2.a) and (3.2.b), we create a new map that shows the space-time correlations in the Lagrangian frame, such as figure (5.3.3). Note that this method of defining a velocity does not cause quadrant symmetry in the Lagrangian map as the band of high correlation could easily have been asymmetrical about the line of least decorrelation. Rather, quadrant symmetry is an expression of the fact that once the effect of the driving upper level winds has been removed, the process in question has, to first order, no preferred direction. Also note that this method for finding the advection velocity may not give the same results as those obtained by tracking the shapes of rain areas. This is because the tracking technique does not take into account the developments inside the rain areas. Furthermore, only the displacements of the rain areas between successive CAPPIs (over 5 min.) determine the advection velocities. The advection velocities obtained from figure (5.3.2) and the like, take into account internal developments as well as displacements over periods longer than 5 minutes. Furthermore, since we are concerned with the structure of space-time correlations, we must define the advection velocity in terms of these correlations. An advection velocity obtained by an area tracking technique is therefore unacceptable since it has an imprecise relationship with the space-time correlations.

In practice, we cannot simply find the Eulerian space-time correlations and then transform the coordinates. This would create a large region in the Lagrangian map where no data is available, as in figure (5.3.3), for example. Instead, we track the motion of the storm system and deduce an overall velocity. The tracking is done using a cross-correlation algorithm which finds the displacement of the general pattern of precipitation between two CAPPIs. Also, in order to reduce the short term fluctuations, previous displacements are weighted into the calculations to find the present displacement between two successive CAPPIs. The result is a sequence of velocities between two succeeding CAPPIs at a given time. The time series of velocities has a definite mean and fluctuations about that mean. Often, the mean itself has a trend, or in other words, an acceleration is apparent. Such an acceleration, even a small one, can affect the space-time correlations by curving the high correlation band. That is why a least-squares fit is performed on the velocity time series, defining an initial velocity, an acceleration and a point standard deviation. The space-time correlations are done relative to the frame moving with that initial velocity and acceleration. The resulting space-time correlation maps are often slanted because the tracking advection velocity does not always agree with the space-time correlation advection velocity. Therefore an adjustment velocity is needed from which we can find the true

Lagrangian space−time correlation

FIG. 5.3.3. The Lagrangian space−time correlations for the convective case on the 19th of June, 1992. Note the symmetry about the 0 km axis for correlations of 0.2 or greater. The dashed line indicates the region where data is not available.

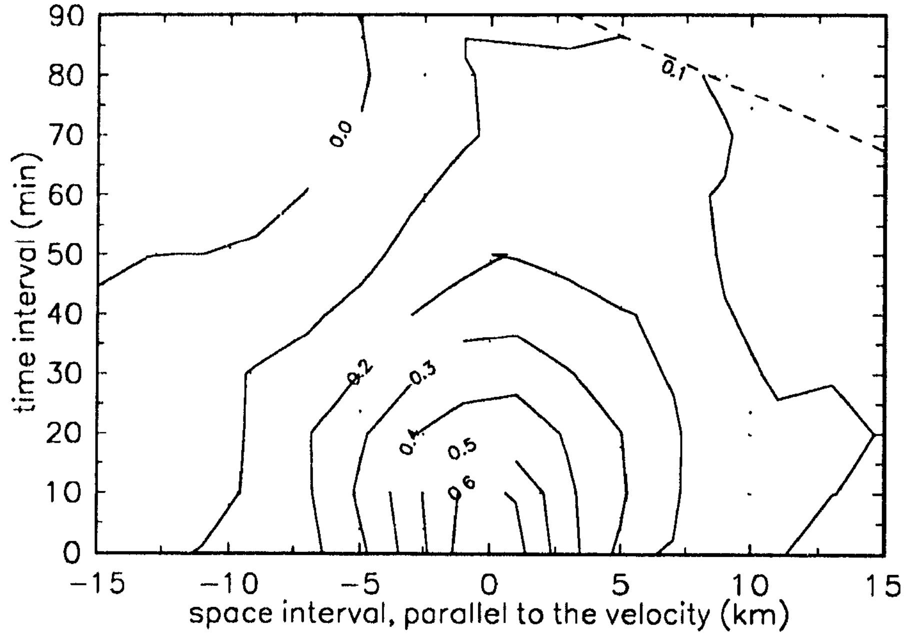

Lagrangian frame. So we have a two stage process for defining an advection velocity, which is the tracking velocity (and acceleration) plus the adjustment velocity. Note that in the cases analyzed, the acceleration is not large and does not induce a large difference in velocity over the duration of the CAPPI sequences relative to the initial velocity. Consequently, the overall advection velocity for a given rain event is taken as the time averaged tracking velocity plus the adjustment velocity.

5.4 Results

In section 3, the notion of space-time isotropy relative to an intrinsic velocity was defined. And in figure (5.3.3), we can see that the correlation contours, in particular 0.2 and greater, can easily be approximated by 'ellipses' in space-time. The quotation marks are to remind the reader that since the axes of the figure represent different physical units, one of them may be rescaled in such a way as to show circles. In a way, it is this rescaling which defines the intrinsic velocity of the system. Furthermore, if the intrinsic velocity may be evaluated, the radial space-time

Intrinsic velocity functions

FIG. 5.4.1 . The intrinsic velocity ($\tilde{U}$), as a function of the time interval ($\tau_{i\rho}$) for the convective case on the 19th of June, 1992. The 0.25, 1 and 2 km resolution CAPPIs are used for the D = 0.5, 1 and 2 km lines respectively, where D is the averaging length.

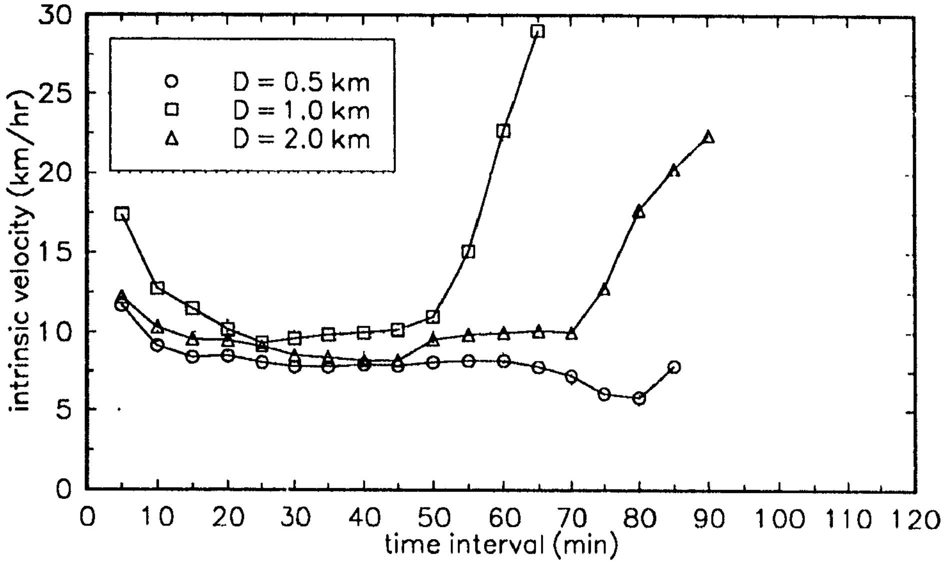

FIG. 5.4.2. The same as in figure (5.4.1) but for the stratiform case on the 31st of July, 1992.

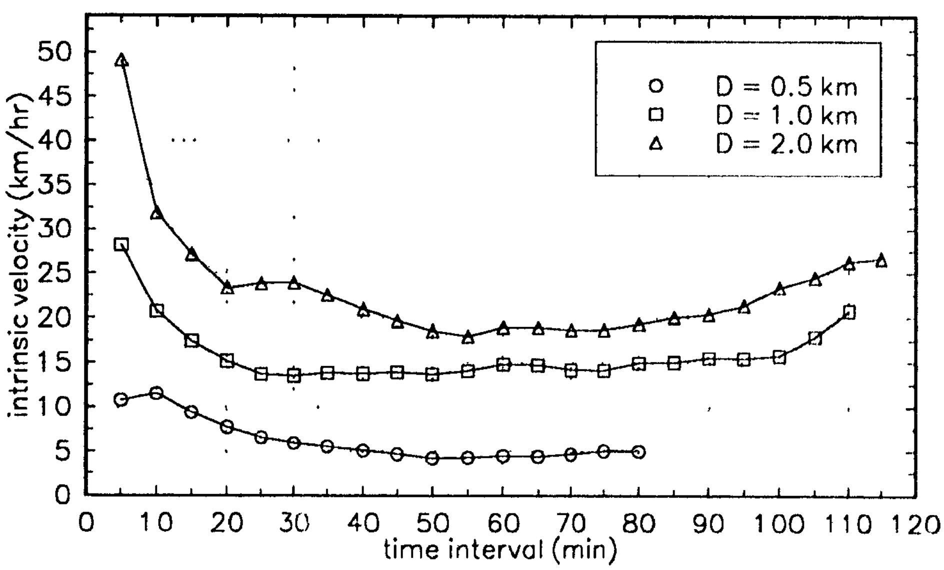

correlation function ($\rho_l(\tau_{l\rho})$, see section 3) may also be found. This leads to a considerable simplification in the representation of the data. Rather than a two-dimensional contour map, which is difficult to read, we have a graph of a one dimensional function coupled with a velocity.

First, we must determine the behaviour of the intrinsic velocity as a function of $\tau_{l\rho}$ to see if it may be approximated as constant. To do so, we find the Lagrangian frame (the line $\overline{OB}$ in figure (3.4)) and for each time interval in that frame, we find the correlation value at that point (points D or B in figure (3.4)). Then we find the point along the space interval axis with the same correlation (figure (3.4); point E given point B) and then take the ratio of the space interval over the time interval. This method should work well if the correlations along the space or Lagrangian time interval axis are not too erratic. Another method was tried where all the points with the same correlation value as the point in the Lagrangian frame (points D or B) are identified and then an ellipse was found that fits the set of points best, the intrinsic velocity being deduced from the shape of the ellipse. However, the results from the ellipse method are not any better than those of the ratio method and so are not shown.

Figures (5.4.1) to (5.4.2) show the results for the two cases. In figure (5.4.1), the results for the convective case on the 19th of June, 1992, are shown. It reveals that the constant velocity hypothesis is a good approximation from 15 min to 70 min for the 500 m resolution data and the 2 km resolution CAPPIs and from 25 min to 50 min for the 1 km resolution CAPPIs. The initial decrease in the intrinsic velocity corresponds well to the result in figure (4.3). The high velocity value at 5 min may be the result of spatial averaging. The dramatic increase at long time intervals may be due to erratic correlations at large displacements. Indeed, as was mentioned in section (5.2) and can be seen in figure (5.3.3), the correlations for large displacements become uncertain since there is less data available to compile statistics. Therefore, the sharp increases for the 1 and 2 km resolution CAPPIs are likely due to spurious correlations along the space or Lagrangian time interval axis. Figure (5.4.2) show the results for the stratiform case on the 31st of July, 1992. Here, the intrinsic velocities are more constant than in the convective case, but the different lines don't seem to converge to the same value (as in figures (4.3) and (5.4.1)). This suggests that the correlations for the stratiform case are more susceptible to the method of data processing than the convective case. Furthermore, no consistent power-law behaviour can be observed from the curves shown (see section 3).

Approximating the intrinsic velocity as constant and assuming the intrinsic and the adjustment (or advection) velocities are known for a given space-time correlation map, the correlation contours should follow the line,

$$\tau(\tau_{l\rho}, \theta) = \tau_{l\rho}\cos(\theta) \tag{5.4.1}$$

$$\alpha(\tau_{l\rho}, \theta, \tilde{U}, \overline{U}) = \tau_{l\rho}[\tilde{U}\sin(\theta) + \overline{U}\cos(\theta)] \tag{5.4.2}$$

where θ is a parameter that describes a position along the contour line, $\tilde{U}$ is the intrinsic velocity and $\overline{U}$ is the adjustment velocity, such as the one discussed previously (or the total advection velocity in the case of figures (3.4) or (5.3.2)). The parameter $\tau_{l\rho}$ is the argument of the radial space-time correlation function (see section 3). Equations (5.4.1) and (5.4.2) therefore describe slanted ellipses such as the ones illustrated in figures (3.4) or (5.3.2).

In practice, we find $\tilde{U}$, $\overline{U}$ and the radial space-time correlation function by making an estimate of the intrinsic and adjustment velocities and choosing a range of values centered around those estimates. For each value of $\tilde{U}$ and $\overline{U}$, we find a corresponding radial space-time correlation function by finding the average correlation along the corresponding slanted ellipse for each value of $\tau_{l\rho}$ (where $-\pi/2 \le \theta \le \pi/2$, owing to the symmetry of the correlation function). In equation form, we have

$$\overline{\rho_l}(\tau_{l\rho}, \tilde{U}, \overline{U}) = \frac{1}{N}\sum_{i=0}^{N} \rho_d[\alpha(\tau_{l\rho}, \theta_i, \tilde{U}, \overline{U}), \tau(\tau_{l\rho}, \theta_i)] \tag{5.4.3}$$

where $\overline{\rho_l}$ can be taken as the radial space-time correlation function obtained from the averaging operation for the given fixed values of $\tilde{U}$ and $\overline{U}$ (i.e. keeping the intrinsic and adjustment velocities constant, it is a function of $\tau_{l\rho}$ only), ρ_d is the space-time correlation map obtained from the data and may require an adjustment velocity to find the Lagrangian frame, and $\theta_i = \pi(i/N - 1/2)$. The number N increases with $\tau_{l\rho}$ in such a way that it is roughly equal to the number of data points of ρ_d that lie on or near the ellipse described by equations (5.4.1-2). The correlation maps taken from actual data consist of a grid of points evenly spaced in time (5 min intervals) and space (variable intervals according to the resolution and rain event). Since it is very unlikely that the data points and sampling points will coincide, the correlation value for the region in between data points is linearly interpolated from those points. Along with the average, we also find the standard deviation of the correlation for each value of $\tau_{l\rho}$.

$$\sigma^2(\tau_{l\rho}, \tilde{U}, \overline{U}) = \frac{1}{N}\sum_{i=0}^{N} \{\rho_d[\alpha(\tau_{l\rho}, \theta_i, \tilde{U}, \overline{U}), \tau(\tau_{l\rho}, \theta_i)] - \overline{\rho_l}(\tau_{l\rho}, \tilde{U}, \overline{U})\}^2 \tag{5.4.4}$$

The standard deviations are then summed over all values of $\tau_{l\rho}$, thus giving a function of $\tilde{U}$ and $\overline{U}$ only.

$$\sigma^2_{total}(\tilde{U},\overline{U}) = \sum_{\tau_{lp}} \sigma^2(\tau_{lp},\tilde{U},\overline{U}) \tag{5.4.5}$$

The values of $\tilde{U}$ and $\overline{U}$ which minimize this sum are taken as the 'real' values as well as the corresponding radial function (i.e. the one obtained from equation (5.4.3) by keeping the velocities constant). The variable τ_{lp} is taken at 5 min intervals, starting at 0 min to two hours (25 values in all). This corresponds to the maximum time interval of the space-time correlation maps and has the effect of excluding the upper left and right-hand corners of the maps. This exclusion removes data that is unreliable. The standard deviations have equal relative weight when summed since the points near $\tau_{lp} = 0$ are stable (because $\overline{\rho_l}(0) = 1$ by definition) but few, while the points at long time intervals are unreliable but numerous. No form of the radial space-time function is assumed beforehand, only a constant intrinsic velocity and the corresponding space-time isotropy. The radial space-time function is free to take any form, exponential, power-law or otherwise, given the isotropy assumption. Note that the radial

Simulated radial space–time correlation functions

FIG. 5.4.3. The radial space–time correlation functions for various averaging lengths (D) from the exponential space–time correlation function with characteristic length L and time T (equation (4.11)).

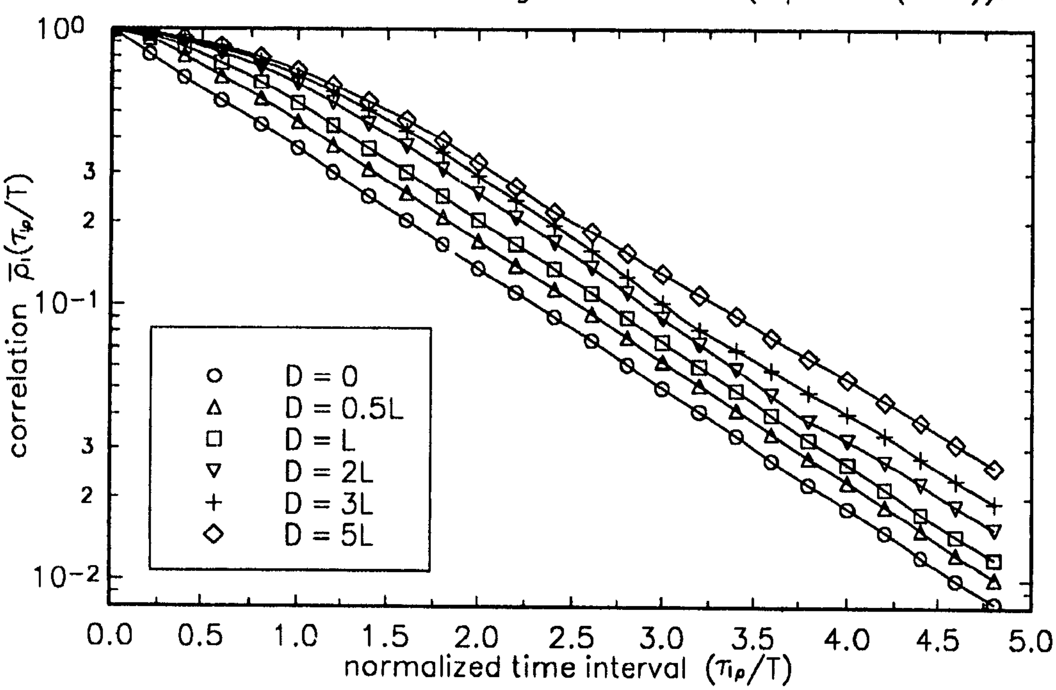

space-time correlation may also be interpreted as a Lagrangian time correlation function which has been smoothed by averaging over space-time correlation map.

We perform this analysis first on the numerical simulation of the exponential space-time correlation function. Although space-time isotropy is no longer strictly true after spatial averaging, we choose to ignore this and treat it as though it were real data. The radial space-time correlation functions for various averaging values of (D/L) is shown in figure (5.4.3). We see a series of curves similar to those in figures (4.1) and (4.2).

The radial space-time correlation functions for various averaging lengths, CAPPI sequences and rain events are shown in figures (5.4.4) to (5.4.9). As a general rule, the correlation increases with increasing averaging length, especially for short time intervals. For the convective case, the radial space-time correlation functions can be approximated by an exponential for the 250 m resolution CAPPI sequence, as well as the 1 km resolution sequence, but not for the 8 km averaging length function from the 2 km resolution sequence. The odd shape of that function may be due to the reduced number of pixels available in the 2 km resolution CAPPIs. Because of the curvature of the earth's surface, the altitude at far ranges is no longer constant but increases with range. Therefore, a maximum radius of 190 km is imposed, instead of 240 km. This does not leave as many pixels available to compile statistics, especially when one considers the large shadow masks used on those CAPPIs. Also, at the 8 km averaging length, the effect of small-scale, high intensity cells on the correlations may be severely impaired, which may in turn affect the statistics. The stratiform case, however, does not decorrelate as rapidly as an exponential and therefore cannot be approximated as such. Rather, there is an initial rapid drop, then a linear decrease with time. There is also a problem with consistency, in that a radial space-time correlation function for a given averaging length obtained from a CAPPI sequence with a given resolution does not always agree with another function for the same averaging length (and rain event) but obtained from a sequence with a different resolution. For example, the functions for D = 1.00 km and D = 2.00 km in figure (5.4.6) decorrelate faster than their counterparts in figure (5.4.4), though it is possible, but unlikely, that this may be due to the difference in altitude. The same holds true for those functions in figure (5.4.7) relative to their counterparts in figure (5.4.5), yet they have the same altitude. Since the radial space-time correlation function may also be taken as the Lagrangian time correlation function, and since the functions for the convective cases are close to being exponential, figures (5.4.14) and (5.4.15) show the 'characteristic' times (i.e. the time interval where the correlation reaches the value e^{-1}) for the radial functions. Those figures summarize the previous figures (5.4.4) to (5.4.9). As expected, the times increase with averaging length, but there is still a

Radial space–time correlation functions

FIG. 5.4.4. The radial space–time correlation functions of the convective case on the 19th of June, 1992, for various averaging lengths D. The CAPPIs have a resolution of 250 m and an altitude of 1.6 km.

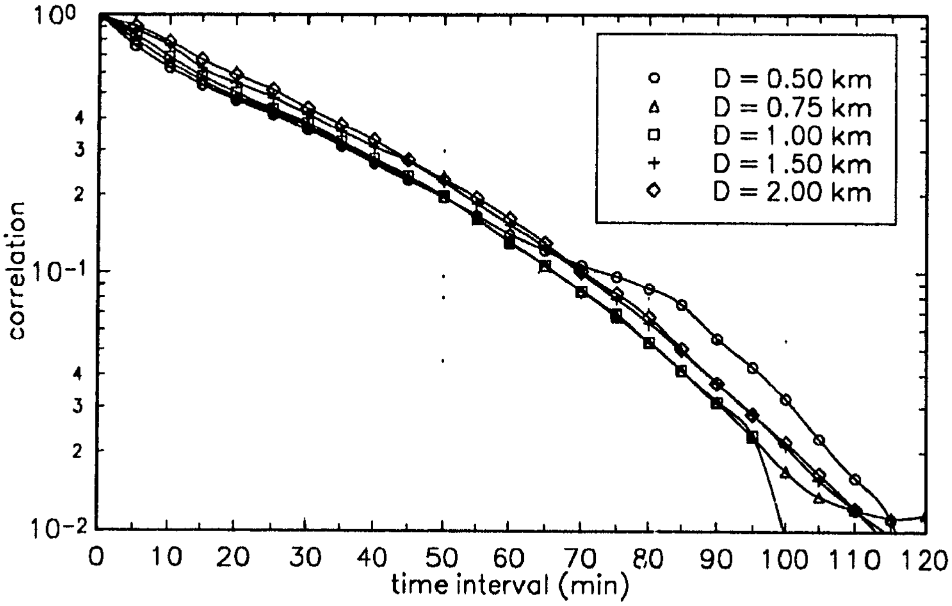

FIG. 5.4.5. The same as in figure (5.4.4) but for the stratiform case on the 31st of July, 1992, with a resolution of 250 m and an altitude of 2.0 km.

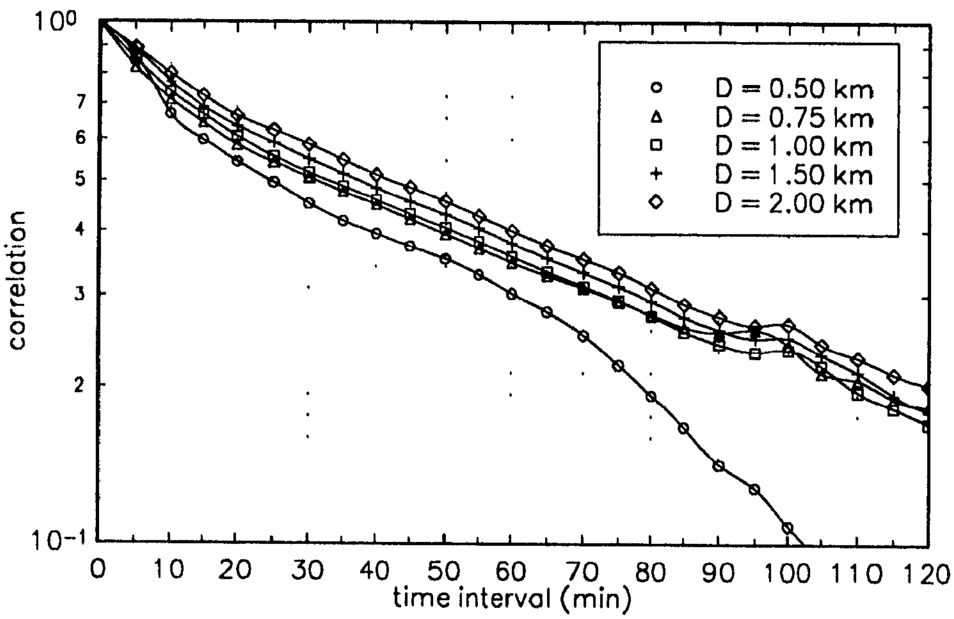

FIG. 5.4.6. The same as in figure (5.4.4) for the convective case, but with a resolution of 1 km and an altitude of 3.0 km.

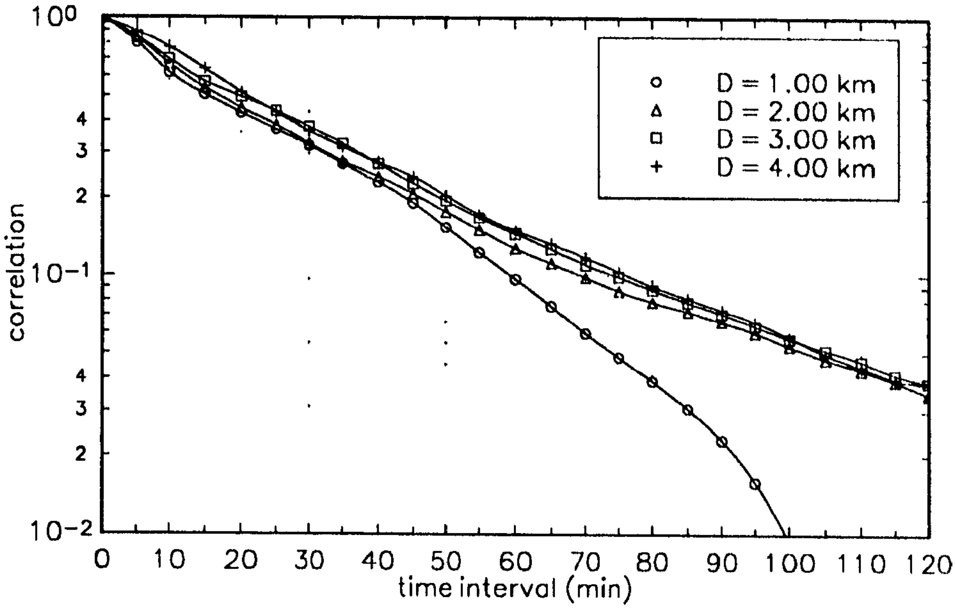

FIG. 5.4.7. The same as in figure (5.4.5) for the stratiform case, but with a resolution of 1 km.

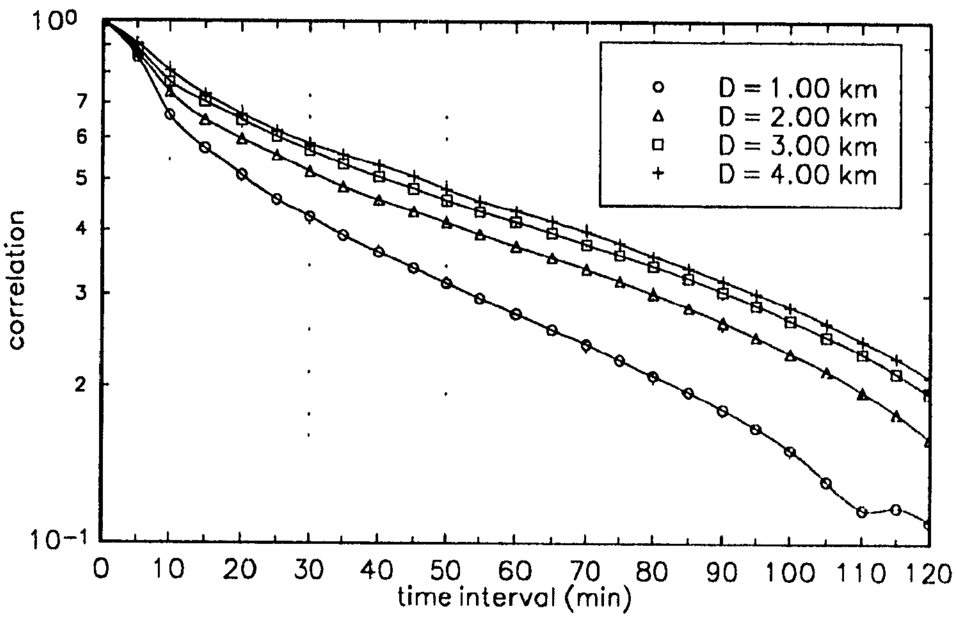

FIG. 5.4.8. The same as in figure (5.4.4) for the convective case, but with a resolution of 2 km and an altitude of 3.0 km.

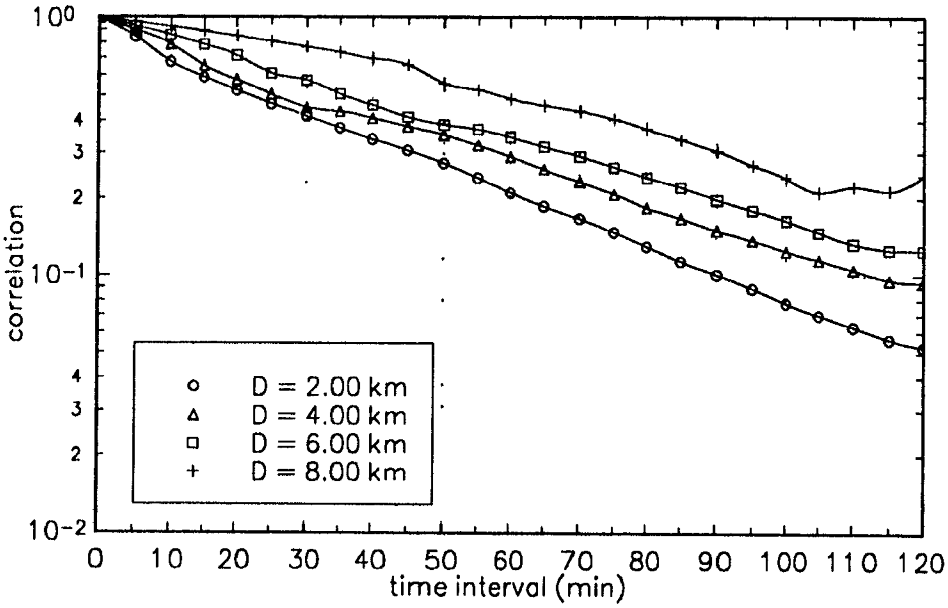

FIG. 5.4.9. The same as in figure (5.4.5) for the stratiform case, but with a resolution of 2 km.

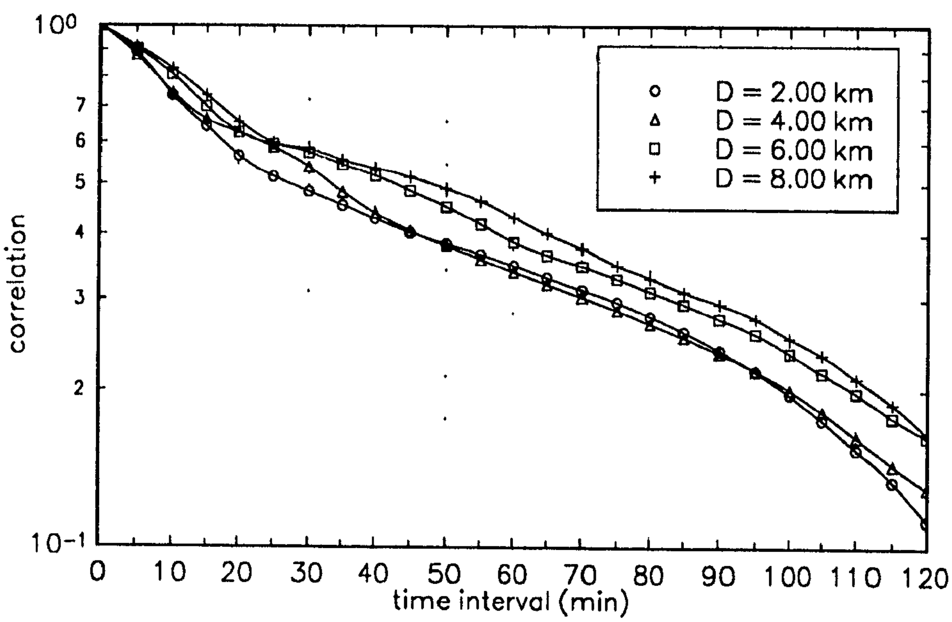

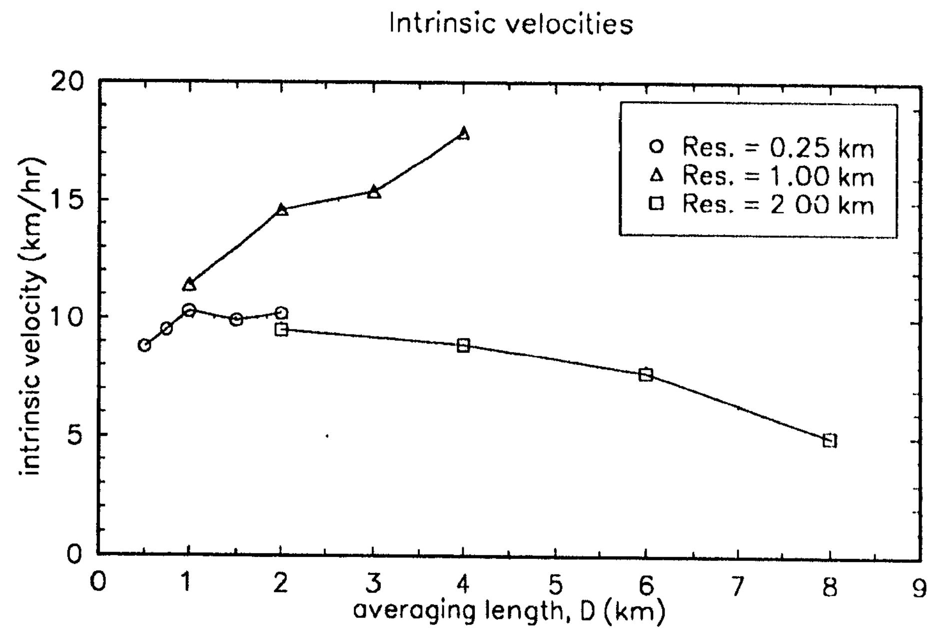

FIG. 5.4.10. The intrinsic velocities of the convective case on the 19th of June, 1992, for various averaging lengths and CAPPI resolutions. The average intrinsic velocity is 11 km/hr.

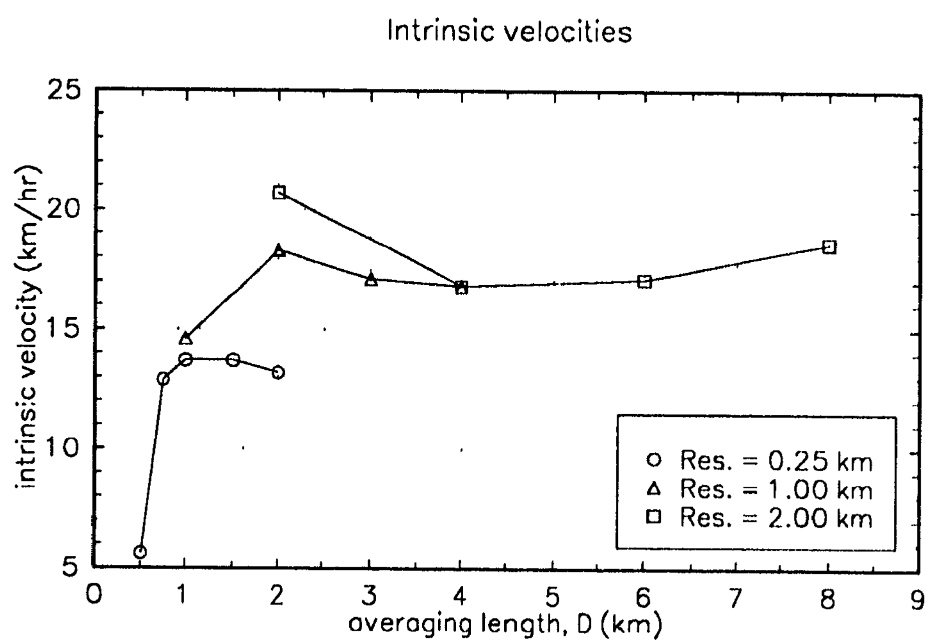

FIG. 5.4.11. The same as in figure (5.4.10) but for the stratiform case on the 31st of July, 1992. The average intrinsic velocity is 15 km/hr.

Advection velocities

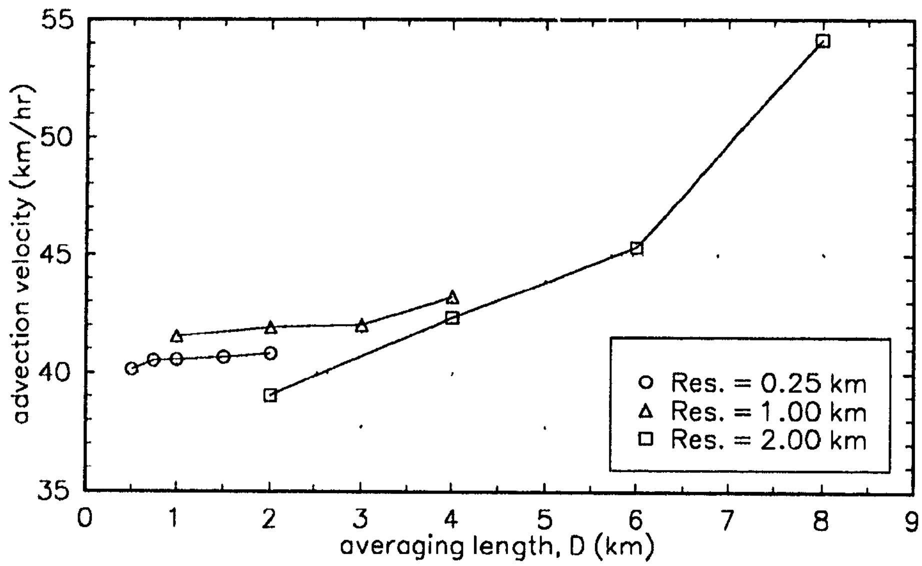

FIG. 5.4.1 2. The same as in figure (5.4.1 0) but for the advection velocities. The average advection velocity is 42 km/hr.

Advection velocities

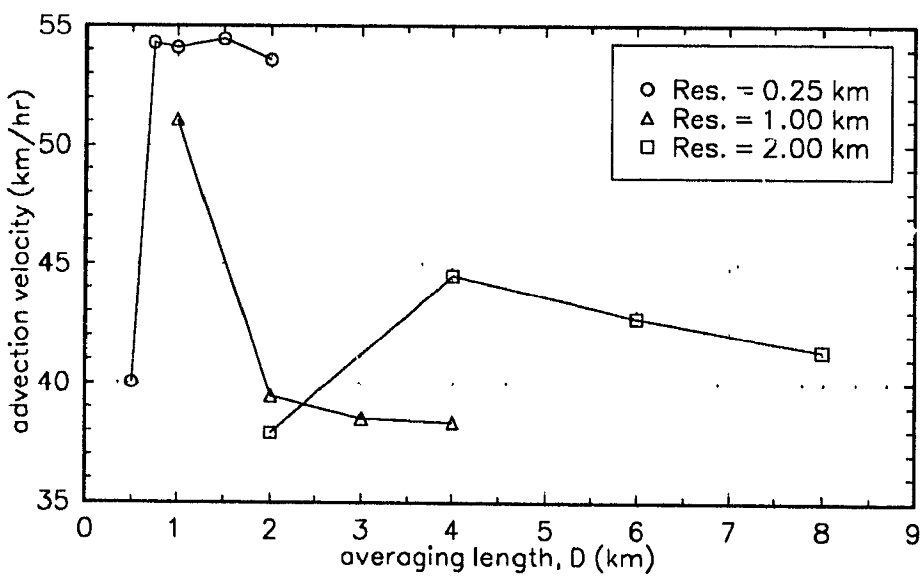

FIG. 5.4.1 3. The same as in figure (5.4.1 1) but for the advection velocities. The average advection velocity is 45 km/hr.

Characteristic times

FIG. 5.4.1 4. Characteristic times ($\rho = 1/e$) of the radial space–time correlation functions for the convective case on the 19th of June, 1992, for various averaging lengths and CAPPI resolutions.

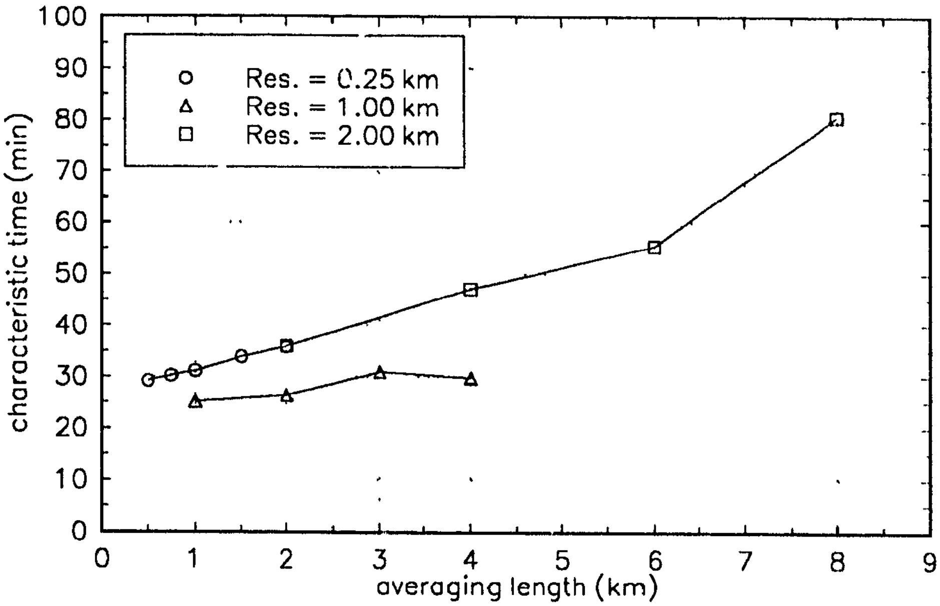

Characteristic times

FIG. 5.4.1 5. The same as in figure (5.4.1 4), but for the stratiform case on the 31 st of July, 1992.

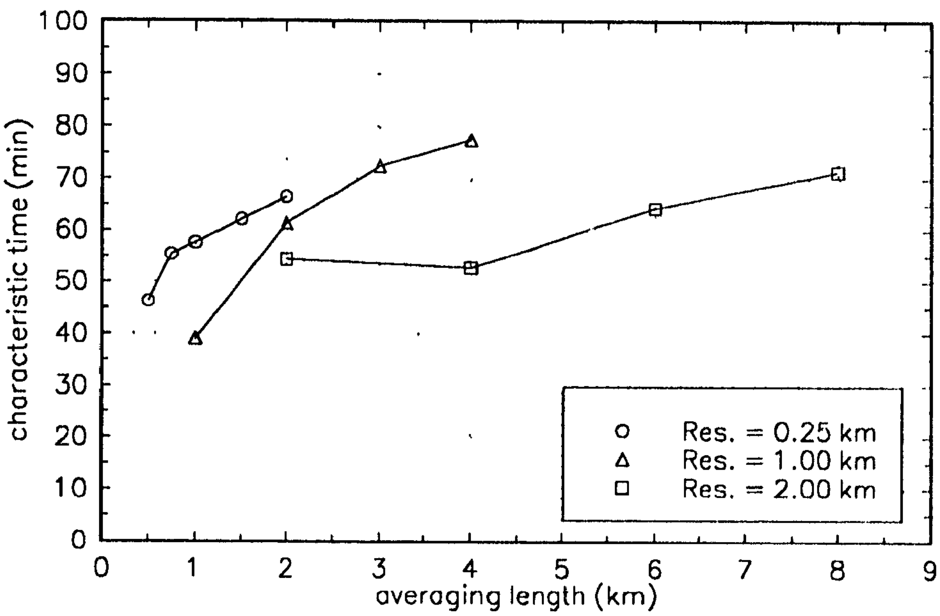

problem with consistency. Note that the meaning of the characteristic times for the stratiform case is somewhat unclear since the shapes of the radial space-time correlation functions are not exponential.

The intrinsic and advection velocities (figures from (5.4.10) to (5.4.13)) do not show a clear relationship with the averaging length. Furthermore, there is again a problem with consistency, for advection as well as intrinsic velocities. In figure (5.4.12), there seems to be an increase of the advection velocity with increasing averaging length and in figure (5.4.13), the advection velocities for the 250 m resolution CAPPIs, except the first one, and the first velocity for the 1 km resolution CAPPIs, seem aberrant with respect to the others. Since we do not expect advection velocities to change with averaging length and since there is no clear relationship for intrinsic velocities, the best we can do to characterize the rain events is to find the average velocities. Consequently, the convective case has an overall intrinsic velocity = 11 ± 3 km/hr, advection velocity = 42 ± 4 km/hr, and the stratiform case has an intrinsic velocity = 15 ± 4 km/hr, advection velocity = 45 ± 7 km/hr. The fact that the intrinsic velocities for the convective and stratiform cases are so close is surprising considering the very different characteristics of these cases. It may be that the spatial and temporal scales change in a similar way from storm to storm, though any conclusions are premature given only two cases.

There are six main factors explaining these discrepancies. The first is the processing of the data used. The method used to measure radar reflectivity and convert it to rainfall for the 1 and 2 km resolution CAPPI sequences is quite different from that used for the 250 m resolution CAPPI sequence. If one method induces greater error in the CAPPIs than the other, then the estimates of the correlation will also contain a greater error. It is possible that the D = 1.00 km and D = 2.00 km functions in figures (5.4.4) and (5.4.6) do not agree for just such a reason. The second factor is a range dependence in the data. This effect can be brought on by a range dependent minimum detectable reflectivity level, or by the fact that the number of radial scans that are averaged to produce one pixel decreases with range. Also, at far ranges, the reflectivity is estimated from a large volume so that any vertical structure of the rainfall affects the estimate as well. The influence of range dependent effects is heightened by the fact that the maximum allowable range for the data changes with averaging length (see section 5.1). The change in maximum allowable range may also introduce precipitation patterns into the data analysis that were not included previously. That should not have too great an influence since for the cases analyzed, the bulk of the precipitation passed over the radar site. Nevertheless, that effect may help to explain the problem with the consistency of the radial space-time correlation functions.

The third factor is the influence of ground clutter and shadows. Ground clutter is a strong return signal coming from an object on the ground such as a mountain range. A shadow is a region of weak or non-existent echoes behind an obstacle (i.e. mountain) which blocks the radar beam. Although both the clutter and the shadows are masked out of the CAPPIs, the clutter has scintillation properties which enable it to protrude out of its masked region. And since the ground clutter often has a much greater reflectivity than rainfall, its effect may be noticeable. The masks for the ground clutter were enlarged precisely for these reasons, but it is difficult to know with certainty the proper extent of the masks without making them excessively large.

The fourth factor is the possible difference in advection velocities between features of different intensities. The greater the averaging length the more the small, high intensity features are attenuated, along with their influence in the determination of an advection velocity. In a study by Lachapelle (1990), it was found that for some storms, the time-averaged advection velocities for regions with 4 mm/hr of rainfall or greater, could be 25% higher than the corresponding advection velocity for regions with 16 mm/hr or greater. In section 5.3, a similar relationship was found for the convective case for rain rate thresholds from 0.5 to 8 mm/hr. The difference in advection velocity between these thresholds is not great and seems insufficient to fully explain the variation of advection velocity with averaging length seen in figure (5.4.12).

The fifth factor may be the assumption of a constant intrinsic velocity itself. We can see in figures (5.4.1) to (5.4.2) that the intrinsic velocity seems constant only over a certain range. The initial drop may be explained by spatial averaging and the final erratic increase may be caused by unreliable statistics. Therefore, the constant intrinsic velocity hypothesis seems reasonable. Nevertheless, the variation of the intrinsic velocity can induce uncertainty in the estimations using equations (5.4.3) and (5.4.4). Note that the form of the radial space-time correlation function for the stratiform case does not resemble an exponential (figures (5.4.5),(5.4.7) and (5.4.9)) which may explain why the intrinsic velocity functions (figure (5.4.2)) do not converge to a common value, as in figure (4.3). This is because figure (4.3) is based on an exponential radial space-time correlation function (equation (4.11)).

The sixth factor may be the imperfections in the algorithm used to find the velocities (i.e. equations (5.4.3-5)). The aberrant advection velocities in figure (5.4.13) (the ones between 50 and 55 km/hr) are very close to the tracking velocity. Given the high value of the tracking velocity, there was a large region on the space-time correlation maps with no data available (figure (5.3.3), for example). In addition, the high-correlation band on those correlation maps were very broad, causing a high level of uncertainty for the adjustment velocity. Under those conditions, the algorithm favors a low adjustment velocity as this would center the ellipses described in equations (5.4.1-2) with respect to the space-time correlation maps. In other words, an adjustment velocity of zero is the best estimate possible given the uncertainty due to the shape of the high-correlation band and the large region of missing data. The broad high correlation bands may be explained by the second and third factors, because these effects do not move. In other words, embedded in the moving rain field is a fixed structure which may diffuse the slant in the space-time correlation function's structure, making the determination of the adjustment velocity more uncertain.

The limitations of the algorithm may also explain the increasing trend of the advection velocities in figure (5.4.12). Specifically, the last two estimates, which account for most of the increasing trend, may be the result of an odd shape of the high-correlation band, in particular the end far from the origin of the space-time correlation map, caused by any or all of the aforementioned factors. This seems all the more plausible given the odd forms of the radial space-time correlation functions for the 6 and 8 km averaging lengths for the convective case (see figure (5.4.8)).

6. Discussion

The dispersion in the estimates of intrinsic and advection velocities, as well as the inconsistency of equivalent radial space-time correlation functions, stand in the way of establishing a relationship between averaging length and space-time correlation structure. As was mentioned previously, the 250 m resolution CAPPIs were obtained using a different data processing method than the 1 or 2 km resolution CAPPIs. From the description, it is not hard to see that the 250 m resolution CAPPIs incorporate much more data than the 1 or 2 km resolution CAPPIs. Consequently, we expect the 250 m resolution method to yield more reliable statistics than the first. A comparison between figures (6.1) and (6.2) seems to confirm this suspicion, since both are supposed to represent the same correlations yet figure (6.2) is 'noisier' than (6.1). This may explain why the radial space-time correlation functions in figures (5.4.6) and (5.4.7) decorrelate faster than their counterparts in (5.4.4) and (5.4.5), respectively. The influence of the error on the rainfall estimates degrades the correlation.

FIG. 6.1. The Eulerian space–time correlations for the stratiform case on the 31st of July, 1992, obtained from the 250 m resolution CAPPIs averaged to a resolution of 1 km. The CAPPIs have an altitude of 2.0 km and cover a region with a 96 km diameter. The dashed contours denote negative correlations.

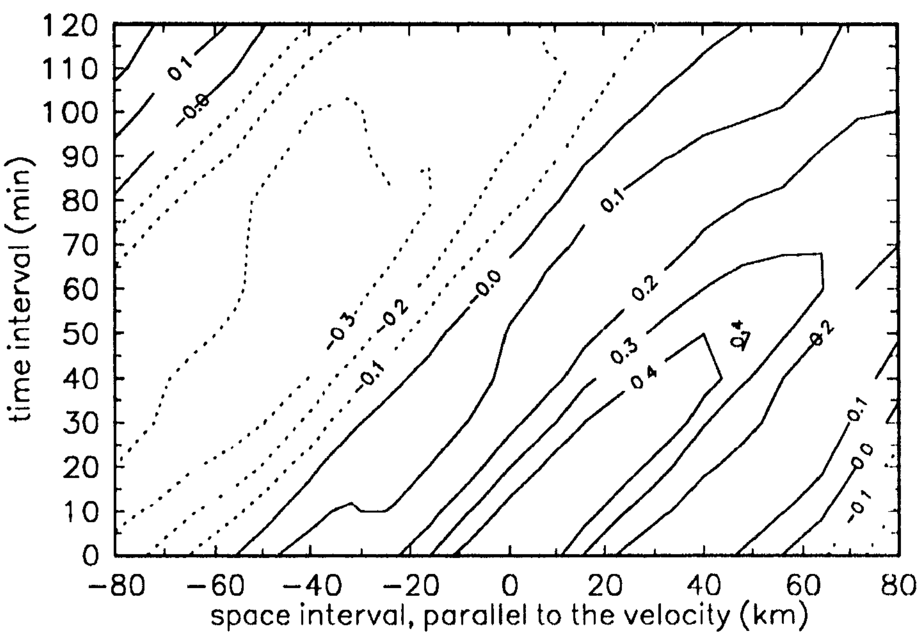

FIG. 6.2. The Eulerian space–time correlations for the same rain event, altitude and region as in figure (6.1), but obtained from 1 km resolution CAPPIs with no averaging. The dashed contours denote negative correlations.

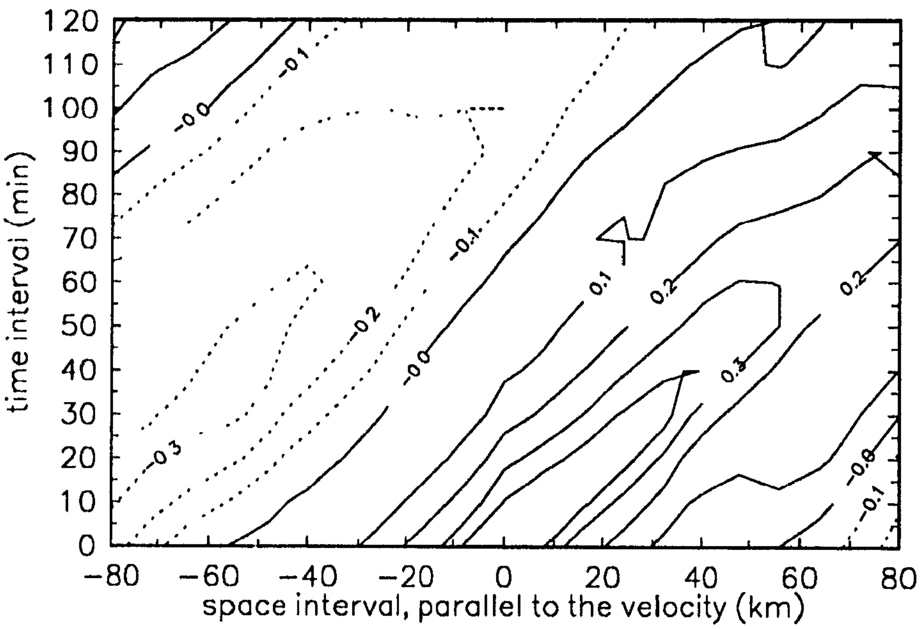

As was pointed out before, the increase in error may render the determination of an advection velocity more difficult, but it may also affect the intrinsic velocity if spatial and temporal statistics are altered differently. On a more fundamental level, there may be limits on the validity of space-time isotropy. While it seems valid for strong correlations, the correlation contours for 0.1 and less can sometimes deviate noticeably from an ellipse. This happens mostly for the 1 and 2 km resolution CAPPIs. Figures (5.4.1) and (5.4.2) demonstrate these points clearly. A less stringent condition would be quadrant symmetry. Instead of averaging the space-time correlations along slanted ellipses, points of the same space interval but with opposite sign (in the Lagrangian frame) can be averaged. Thus we would obtain a two-dimensional correlation map showing only positive time and (Lagrangian) space intervals, which is not as smooth or convenient as a one-dimensional function.

The scale-dependent intrinsic velocity suggested by Lovejoy & Schertzer (1991), (1992) and Tessier et al. (1993), cannot be confirmed for the two cases analyzed. One must be careful when interpreting the data, however. The power-law form suggested for the intrinsic velocity function requires data over many orders of magnitude to be properly analyzed. This is not the case here since the minimum time interval is 5 min and the maximum 120 min. In addition, not all of that range is reliable or even contains a value of the intrinsic velocity. Furthermore, it is possible that the spatial averaging of the data obscures the power-law form for short time intervals. Be that as it may, for the cases observed, a power-law with an exponent of 1/2 for the intrinsic velocity seems unlikely, rather a constant intrinsic velocity is the most reasonable, and simplest, assumption. We may question the reasoning that lead to the formulation of the scale-dependent intrinsic velocity hypothesis. Tessier et al. (1993) reasoned that since the atmosphere is turbulent and exhibits scaling behaviour all through the mesoscale range, no large-scale forcing can be invoked in order to provide an overall advection velocity. Turbulent does not mean completely random, however. It is well known that mid-latitude storm systems have a marked tendency to travel from west to east. There may be a north-south component to the motion, and occasionally a storm system may move from east to west, though its velocity would be greatly reduced. It therefore seems likely that on the whole, storm systems at mid-latitudes have an average velocity towards the east. This is most likely the product of the global circulation between the equator and the poles and the Coriolis force. Surely, this constitutes a large-scale forcing.

The consequences for Taylor's hypothesis are slight for the two cases studied, however. If we assumed an intrinsic velocity of 20 km/hr and an advection velocity of 40 km/hr, which is well above any observed velocity ratio, then equation (3.18) yields a space-time conversion factor of $U'' = \sqrt{U^2 + \tilde{U}^2} \approx 45$ km/hr. The difference of 5 km/hr between this and the advection velocity is close to or within the uncertainty for the advection velocity (±4 km/hr for the convective case and ±7 km/hr for the stratiform case). This means that unless the intrinsic velocity is comparable to the advection velocity, the improvement made to Taylor's hypothesis would not be significant when compared to the error on the advection velocity. Add to this the error on the Eulerian time and space correlations at large displacements and the fluctuations of the intrinsic velocity, and the significance of the improvement is reduced even further. Figure (6.3) shows a limited improvement on Taylor's hypothesis, which is by no means the rule. In it we can see that the modified space-time conversion factor, U'', applied to the Eulerian spatial correlation function, produces a curve that is closer to the temporal Eulerian correlation function than the one obtained using simply the advection velocity. Thereby implying that we can obtain a better estimate of the spatial correlations from the temporal correlations by incorporating the

An example of Taylor's hypothesis

FIG. 6.3. The Eulerian temporal correlations for the case on the 31 st of July, 1992, with a 2 km averaging length from the 1 km resolution CAPPIs, compared with the Eulerian spatial correlations transformed using the advection velocity (39.5 km/hr) and the modified velocity (43.5 km/hr). The intrinsic velocity is 18.3 km/hr.

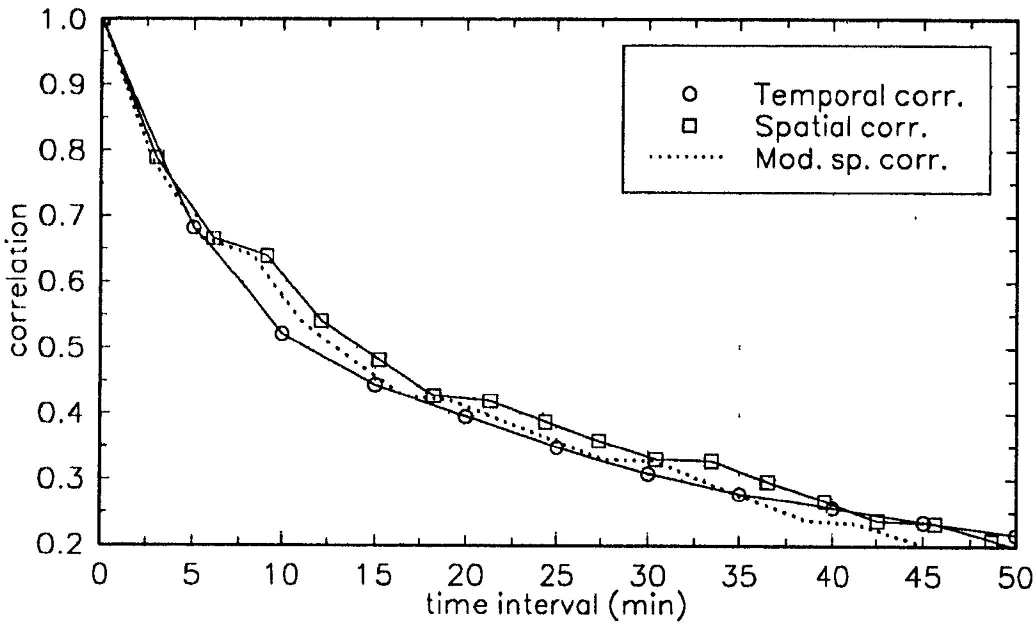

intrinsic velocity in the space-time conversion. However, we can also see that the difference is not great and could easily have been overwhelmed by the error on the two correlation functions or the velocities.

The consequences for Taylor's hypothesis are slight with respect to spatial resolution as well. Since the characteristic times in figures (5.4.14) and (5.4.15) can be taken as estimates for the variable T in equation (3.13) and since we know the intrinsic and advection velocities from figures (5.4.10) to (5.4.13), we can estimate the cut-off times for Taylor's hypothesis divided by the maximum error (τ_c/ε_m), using equation (3.13). Note that equation (3.13) is not as accurate for the stratiform case since it assume an exponential radial space-time correlation function. Nevertheless, figure (6.3) justifies the use of that equation since a direct estimation is too unreliable given the errors on the correlation. Figures (6.4) and (6.5) show these estimates. Note that since the cut-off times are divided by the maximum error, which must be much less than one for equation (3.13) to hold (i.e. $\varepsilon_m \approx 0.1 - 0.01$), a value of 1000 minutes may in fact indicate a cut-off time between 10 to 100 minutes. In figure (6.4), we see that the upper line has an

Cut-off times

FIG. 6.4. The cut-off times for Taylor's hypothesis divided by the maximum error (τ_c/ε_m) as a function of averaging length (D) for the convective case on the 19th of June, 1992.

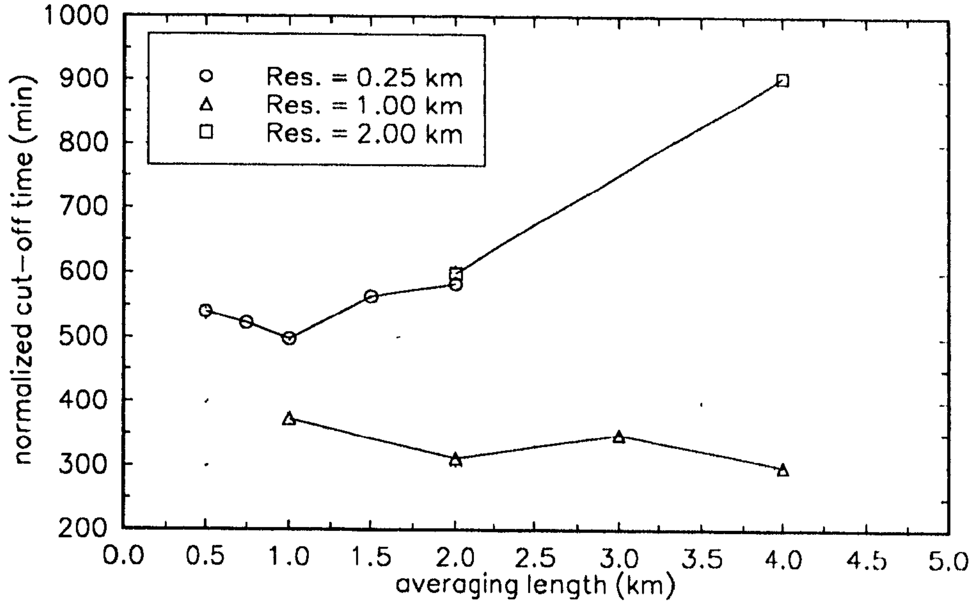

Cut-off times

FIG. 6.5. The same as in figure (6.4) but for the stratiform case on the 31st of July, 1992.

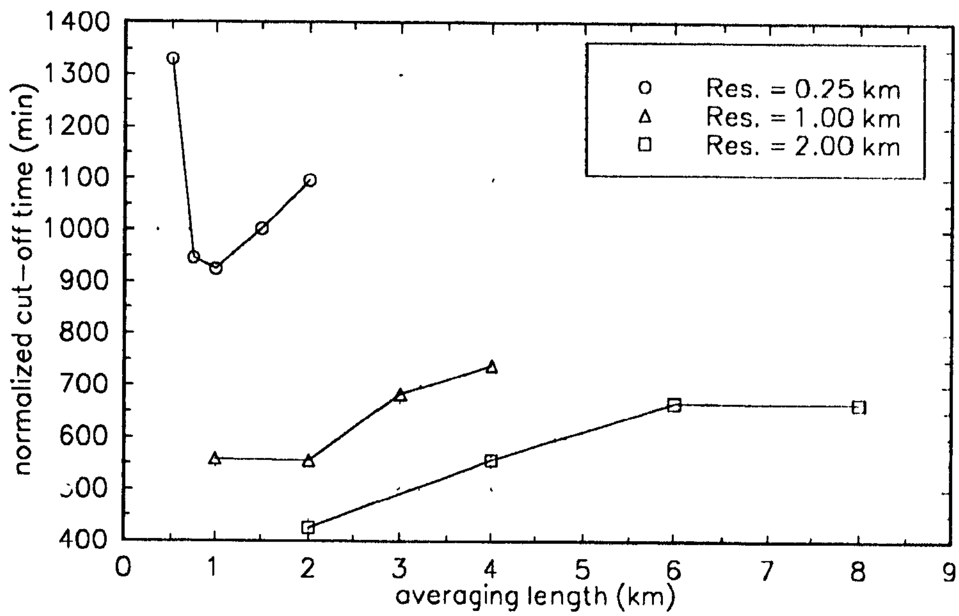

increasing trend but the lower one does not while as in figure (6.5), no trend is immediately apparent. Note that the values for the 6 and 8 km averaging lengths in figure (6.4) were omitted as they were excessively high due to the anomalous shape of the corresponding radial space-time correlation functions. Although the characteristic times increase with averaging length, implying a greater persistence of the features of the averaged field, there seems to be no definite relation between the cut-off times and the averaging lengths due to the uncertainty on the advection and intrinsic velocities.

We may conclude that for the cases seen here, the 'frozen turbulence' model is still a reasonably good approximation for Taylor's hypothesis. Only for cases that are slow moving and show a great deal of internal development during their passage would the intrinsic velocity introduce a significant improvement for Taylor's hypothesis. Moreover, spatial resolution does not alter the validity of Taylor's hypothesis in any decided way due mainly to the uncertainty on the estimation of the velocities. Indeed, simply finding the proper advection velocity constitutes in itself the main source of error for Taylor's hypothesis.

7. Conclusion

In order to analyze the space-time correlation structure of a particular rain event, the existence of a Lagrangian reference frame moving with the overall motion of the storm is assumed. In this frame, the storm is modelled by a homogeneous and stationary random field whose space-time correlation function is symmetric with respect to a change of sign of the Lagrangian space interval. This is called quadrant symmetry and expresses the fact that in the Lagrangian frame there is no overall motion of any storm element.

Further, the Lagrangian space-time correlations may be approximated as space-time isotropic with respect to a certain velocity. In other words, if the time interval axis of the space-time correlation function were transformed into a space interval axis by means of a given velocity and the resulting correlation function were isotropic, then we have space-time isotropy relative to that velocity. For a rain event this is called the intrinsic velocity and represents the internal kinematic activity of the storm. An alternative is discussed whereas the intrinsic velocity changes with the time interval in the Lagrangian frame. Accordingly, the intrinsic velocity would vary as the time interval to the power of 1/2.

If the intrinsic velocity is assumed to be constant, then the Lagrangian space-time correlation function can be made isotropic and reduced to a radial correlation function. The space-time correlations can now be reduced to three elements; the advection velocity, the intrinsic velocity and a radial space-time correlation function. The spatial and temporal correlations in the Eulerian (fixed) frame can be reconstructed using these elements. The validity of Taylor's hypothesis can also be assessed using these elements. For instance, if the argument of the radial correlation function was made to have units of time, then the cut-off time for Taylor's hypothesis can be expressed as a function of a time interval characterizing the function, a dimensionless error coefficient and the ratio of the intrinsic velocity with respect to the advection velocity. This was done for an idealized exponential Lagrangian space-time correlation function. Taylor's hypothesis can be improved so as to take into account the internal development of a storm system. This is done by incorporating the intrinsic velocity into its formulation (see equations (3.21) and (3.22)).

The effect of spatial averaging on the space-time correlation function is determined theoretically to simulate the effect of the variable resolution of radar data. A numerical estimation of this effect is performed on the exponential space-time correlation function. The spatial averaging increases the intrinsic velocity at short time intervals but does not alter it for arbitrarily long intervals. The radial space-time correlation function, obtained by assuming space-time isotropy (i.e. constant intrinsic velocity), increases its correlation value by a multiplicative factor greater than one in the long time interval region.

Two rain events, a convective case on the 19th of June, 1992, and a stratiform case on the 31st of July, 1992, were recorded and analyzed over spatial resolutions ranging from 500 m to 8 km. The radial space-time correlation functions for the convective case resemble exponential decay functions whose correlation value increases with resolution in a manner similar to the idealized exponential function. The stratiform case has radial functions with an initial rapid drop and then a linear decrease of correlation. The correlation value of those functions also increases with spatial resolution. The intrinsic velocities for both cases can be approximated as constant over a certain range of the time interval. The stratiform case shows intrinsic velocities that are approximately constant over a longer range than the convective case, but the value of those velocities changes with resolution in a manner not consistent with the theoretical result found in section (4). This may be an effect of the data processing or the structure of the space-time correlations or both. The power-law dependence of the intrinsic velocity with time interval cannot be observed. There is uncertainty regarding the relationship of the intrinsic and advection velocities with spatial resolution. The best that can be done is to find the average value of these quantities and assume the effect of spatial resolution to be negligible. For the convective case, the intrinsic velocity is of the order 11 ± 3 km/hr and the advection velocity, 42 ± 4 km/hr. For the stratiform case, the intrinsic velocity is of the order 15 ± 4 km/hr and the advection velocity, 45 ± 7 km/hr. The values of the advection and intrinsic velocities, along with the errors for these velocities, do not allow a meaningful improvement on Taylor's hypothesis as well as a clear determination of the effect of spatial resolution on its validity. The 'frozen turbulence' model is still a good approximation for the cases analyzed given that the uncertainties on the advection velocity and on the correlations, are sufficient to overwhelm any improvement on Taylor's hypothesis.

Appendix A : Accelerated Taylor's hypothesis

When a homogeneous and stationary random field is advected past fixed coordinate system with a constant acceleration, that acceleration induces nonstationarity in the fixed frame. Taylor's hypothesis can still be defined in this context with the following modifications.

Given the Lagrangian coordinates (x_l, t_l) and the Eulerian coordinates (x_e, t_e), the transformation of coordinates is

$$t_e = t_l \tag{A.1}$$

$$x_l = x_e - U_0(t_e - t_{e0}) - \frac{1}{2}a(t_e - t_{e0})^2 \tag{A.2}$$

where U_0 is the velocity at time t_{e0} and a is the acceleration. Due to equation (A.1) we will drop the subscripts when referring to time. Also, equation (A.2) assumes $x_l = x_e$ when $t = t_0$. We can simplify equation (A.2) by setting $t_0 = 0$.

$$x_l = x_e - U_0 t - \frac{1}{2}a t^2 \tag{A.3}$$

In the Lagrangian frame, the spatial interval of the points $P_1(x_{l1}, t_1)$ and $P_2(x_{l2}, t_2)$ transforms into the Eulerian spatial interval by the following equations.

$$x_{l2} - x_{l1} = x_{e2} - x_{e1} - U_0 t_2 + U_0 t_1 - \frac{1}{2}a t_1^2 + \frac{1}{2}a t_2^2 \tag{A.4}$$

$$x_{l2} - x_{l1} = x_{e2} - x_{e1} - U_0(t_2 - t_1) - \frac{1}{2}a(t_2 + t_1)(t_2 - t_1) \tag{A.5}$$

$$\alpha_l = \alpha_e - (U_0 + a\bar{t})\tau \tag{A.6}$$

where α and τ are space and time intervals respectively, and $\bar{t} = (t_1 + t_1)/2$ is the average time. When $\bar{t}$ is kept constant, we can define the velocity $U' = U_0 + a\bar{t}$ which gives the transformation

$$\alpha_l = \alpha_e - U'\tau \tag{A.7}$$

This is the space to time relationship needed to define Taylor's hypothesis. Therefore, the nonstationarity caused by the acceleration can be hidden by choosing a fixed average time.

Appendix B : Relationship between the correlation functions

The correlation function where the mean was subtracted from the field, $\rho(\alpha,\beta,\tau)$, and the one where the mean is not subtracted, $C(\alpha,\beta,\tau)$, are related by an approximate linear relationship.

We start by finding the covariance function,

$$\mathrm{Cov}(\alpha,\beta,\tau)=\frac{1}{A'T'}\sum_{i',j',k'}[R(x_{i'}+\alpha,y_{j'}+\beta,t_{k'}+\tau)-<R>]\times[R(x_{i'},y_{j'},t_{k'})-<R>] \qquad (B.1)$$

where $A'T'$ is the subarea within the total space-time area AT that contains all starting points for the space-time displacement vector such that the end points are also contained in AT. Similarly, the mean $<R>$ is defined as,

$$<R>=\frac{1}{AT}\sum_{i,j,k}R(x_i,y_j,t_k) \qquad (B.2)$$

where $< >$ denotes an averaging operation over AT. Expressing the product of the square brackets in equation (B.1) as a polynomial, we obtain

$$\mathrm{Cov}(\alpha,\beta,\tau)=\frac{1}{A'T'}\sum_{i',j',k'}[R(x_{i'}+\alpha,y_{j'}+\beta,t_{k'}+\tau)R(x_{i'},y_{j'},t_{k'})$$

$$-R(x_{i'}+\alpha,y_{j'}+\beta,t_{k'}+\tau)<R>-<R>R(x_{i'},y_{j'},t_{k'})+<R>^2] \qquad (B.3)$$

We perform the averaging operation on each term separately.

$$\mathrm{Cov}(\alpha,\beta,\tau)=<R(x_{i'}+\alpha,y_{j'}+\beta,t_{k'}+\tau)R(x_{i'},y_{j'},t_{k'})>'-<R(x_{i'}+\alpha,y_{j'}+\beta,t_{k'}+\tau)>'<R>$$

$$-<R><R(x_{i'},y_{j'},t_{k'})>'+<R>^2 \qquad (B.4)$$

where $< >'$ denotes averaging over $A'T'$. As $\alpha,\beta,\tau\rightarrow 0$, we have $<R(x_{i'}+\alpha,y_{j'}+\beta,t_{k'}+\tau>'\rightarrow<R>$ and $<R(x_{i'},y_{j'},t_{k'})>'\rightarrow<R>$. So for sufficiently small space-time displacements, we can approximate equation (B.4) as,

$$\mathrm{Cov}(\alpha,\beta,\tau)=<R(x_{i'}+\alpha,y_{j'}+\beta,t_{k'}+\tau)R(x_{i'},y_{j'},t_{k'})>'-<R>^2 \qquad (B.5)$$

The correlation functions are defined as,

$$\rho(\alpha,\beta,\tau)=\frac{\mathrm{Cov}(\alpha,\beta,\tau)}{\sigma^2} \quad \text{where} \quad \sigma^2=<R^2>-<R>^2 \qquad (B.6)$$

and

$$C(\alpha,\beta,\tau)=\frac{<R(x_{i'}+\alpha,y_{j'}+\beta,t_{k'}+\tau)R(x_{i'},y_{j'},t_{k'})>'}{<R^2>} \qquad (B.7)$$

Substituting equations (B.6) and (B.7) into (B.5) we obtain,

$$\sigma^2\rho(\alpha,\beta,\tau)=<R^2>C(\alpha,\beta,\tau)-<R>^2 \qquad (B.8)$$

Therefore, by isolating $C(\alpha,\beta,\tau)$ and for sufficiently small space-time displacements, we obtain a linear relationship between the two types of correlation functions identical to equation (5.2.9).

$$C(\alpha,\beta,\tau)=\left(\frac{\sigma^2}{<R^2>}\right)\rho(\alpha,\beta,\tau)+\frac{<R>^2}{<R^2>} \qquad (B.9)$$

Bibliography

Adler, R. F., and R. A. Mack, 1984: Thunderstorm cloud height-rainfall rate relations for use with satellite rainfall estimation techniques. *J. Climate Appl. Meteor.*, **23**, 280-296.

Antonia, R. A., A. J. Chambers and N. Phan-Thien, 1980: Taylor's hypothesis and spectra of velocity and temperature derivatives in a turbulent shear flow. *Boundary-Layer Meteorology*, **19**, 19-29.

Atlas, D., D. Rosenfeld and D. A. Short, 1990: The estimation of convective rainfall by area integrals 1. The theoretical and empirical basis. *J. Geophys. Res.*, **95**, 2153-2160.

Bell, T. L., 1987: A space-time stochastic model of rainfall for satellite remote sensing studies. *J. Geophys. Res.*, **92**, 9631-9643.

Biondini, R., 1976: Cloud motion and rainfall statistics. *J. Appl. Meteor.*, **15**, 205-224.

Cahalan, R. F., and J. H. Joseph, 1989: Fractal statistics of cloud fields. *Mon. Wea. Rev.*, **117**, 261-272.

Cates, M. E., and J. M. Deutsch, 1987: Spatial correlations in multifractals. *Phys. Rev. A.*, **35**, 4907-4910.

Crane, R. K., 1990: Space-time structure of rain rate fields. *J. Geophys. Res.*, **95**, 2011-2020.

Dennis, A. S., and F. G. Fernald, 1963: Frequency distribution of shower sizes. *J. Appl. Meteor.*, **2**, 767-769.

Drufuca, G., and I. I. Zawadzki, 1975: Statistics of raingage data. *J. Appl. Meteor.*, **14**, 1419-1429.

Drufuca, G., 1977: Radar-derived statistics on the structure of precipitation patterns. *J. Appl. Meteor.*, **16**, 1029-1035.

Gupta, V. K., and E. Waymire, 1987: On Taylor's hypothesis and dissipation in rainfall. *J. Geophys. Res.*, **92**, 9657-9660.

Gupta, V. K., and E. Waymire, 1990: Mutliscaling properties of spatial rainfall and river flow distributions. *J. Geophys. Res.*, **95**, 1999-2009.

Gupta, V. K., and E. Waymire, 1993: A statistical analysis of mesoscale rainfall as a random cascade. *J. Appl. Meteor.*, **32**, 251-267.

Hentschel, H. G. E. and I. Procaccia, 1984: Relative diffusion in turbulent media: The fractal dimension of clouds. *Phys. Rev. A.*, **29**, 1461-1470.

Heskestad, G., 1965: A generalized Taylor hypothesis with application for high Reynolds number shear flows. *Trans. ASME, J. Appl. Mech.*, **87**, 735-739.

Lachapelle, J., 1990: Propriétés statistiques de la précipitation. M.Sc. thesis, Université du Québec à Montréal, Montréal, Canada.

Laughlin, C. R., 1981: On the effect of temporal sampling on the observation of mean rainfall, Precipitation Measurements From Space, Workshop report, edited by D. Atlas and O. W. Thiele, *NASA publ.*, Goddard Space Flight Center, Greenbelt, Md.

Lee, S. J. and T. C. Halsey, 1990: Some results on multifractal correlations. *Physica A*, **164**, 575-592.

Lopez, R. E., 1976: Radar characteristics of the cloud populations of tropical disturbances in the Northwest Atlantic. *Mon. Wea. Rev.*, **104**, 268-283.

Lopez, R. E., 1977: The lognormal distribution and cumulus cloud populations. *Mon. Wea. Rev.*, **105**, 865-872.

Lovejoy, S., 1982: Area-perimeter relation for rain and cloud areas. *Science*, **216**, 185-187.

Lovejoy, S., and B. B. Mandelbrot, 1985: Fractal properties of rain, and a fractal model. *Tellus*, **37A**, 209-232.

Lovejoy, S., and D. Schertzer, 1985: Generalized scale invariance in the atmosphere and fractal models of rain. *Water Resour. Res.*, **21**, 1233-1250.

Lovejoy, S., and D. Schertzer, 1990: Multifractals, universality classes and satellite and radar measurements of cloud and rain fields. *J. Geophys. Res.*, **95**, 2021-2034.

Lovejoy, S., and D. Schertzer, 1991: Multifractal analysis techniques and rain and cloud fields from 10^{-3} to 10^{6} m. *Scaling, Fractals and Non-linear Variability in Geophysics*, D. Schertzer, S. Lovejoy eds, 111-144, Kluwer.

Lovejoy, S., and D. Schertzer, 1992: Multifractals and rain. *New Uncertainty Concepts in Hydrology and Water Resources*, Z. W. Kunzewicz, Ed., Cambridge University Press.

Marshall, J. S., 1971: Peak reading and thresholding in processing radar weather data. *J. Appl. Meteor.*, **10**, 1213-1223.

Marshall, J. S., and W. Hitschfeld, 1953: Interpretation of the fluctuating echo from randomly distributed scatterers. Part I. *Can. J. Phys.*, **31**, 962-994.

Meneveau, C., and A. B. Chhabra, 1990: Two-point statistics of multifractal measures. *Physica A*, **164**, 564-574.

Mejía, J. M., and I. Rodríguez-Iturbe, 1974: On the synthesis of random field sampling from the spectrum: An application to the generation of hydrologic spatial processes. *Water Resour. Res.*, **10**, 705-711.

Nakamoto, S., J. B. Valdés and G. R. North, 1990: Frequency-wavenumber spectrum for GATE phase I rainfields. *J. Appl. Meteor.*, **29**, 842-850.

Rodríguez-Iturbe, I., and J. M. Mejía, 1974a: The design of rainfall networks in time and space. *Water Resour. Res.*, **10**, 713-728.

Rodríguez-Iturbe, I., and J. M. Mejía, 1974b: On the transformation of point to areal rainfall. *Water Resour. Res.*, **10**, 729-735.

Rosenfeld, D., D. Atlas and D. A. Short, 1990: The estimation of convective rainfall by area integrals 2. The height-area rainfall threshold (HART) method. *J. Geophys. Res.*, **95**, 2161-2176.

Schertzer, D., S. Lovejoy, 1987: Physical modeling and analysis of rain and clouds by anisotropic scaling multiplicative processes. *J. Geophys. Res.*, **92**, 9693-9714.

Seed, A. W., 1989: Statistical problems in measuring convective rainfall. Ph.D. Thesis, McGill University, Montréal, Canada.

Short, D. A., and G. R. North, 1990: The beam filling error in the Nimbus 5 electronically scanning microwave radiometer observations of Global Atlantic Tropical Experiment Rainfall. *J. Geophys. Res.*, **95**, 2187-2193.

Siebesma, A. P., and L. Pietronero, 1988: Correlations in multifractals. *J. Phys. A. Math. Gen.*, **21**, 3259-3267.

Taylor, G. I., 1938: The spectrum of turbulence. *Proc. R. Soc. London, Ser. A.*, **164**, 476-490.

Tessier, Y., S. Lovejoy, and D. Schertzer, 1993: Universal multifractals: Theory and observations for rain and clouds. *J. Appl. Meteor.*, **32**, 223-250.

Vanmarcke, E., *Random Fields: Analysis and Synthesis*, MIT Press, Cambridge, Mass., 1983.

Wallace, P. R., 1953: Interpretation of the fluctuating echo from randomly distributed scatterers. Part II. *Can. J. Phys.*, **31**, 995-1009.

Waymire, E., 1985: Scaling limits and self-similarity in precipitation fields. *Water Resour. Res.*, **21**, 1271-1281.

Waymire, E., V. K. Gupta and I. Rodriguez-Iturbe, 1984: A spectral theory of rainfall intensity at the meso-β scale. *Water Resour. Res.*, **20**, 1453-1465.

Whittle, P., 1954: On stationary processes in the plane. *Biometrika*, **41**, 434-449.

Wyngaard, J. C., and S. F. Clifford, 1977: Taylor's hypothesis and high-frequency turbulence spectra. *J. Atmos. Sci.*, **34**, 922-929.

Zawadzki, I. I., 1972: Statistical studies of radar precipitation patterns. Ph.D. Thesis, McGill University, Montréal, Canada.

Zawadzki, I. I., 1973a: Statistical properties of precipitation patterns. *J. Appl. Meteor.*, **12**, 459-472.

Zawadzki, I. I., 1973b: The loss of information due to finite sample volume in radar-measured reflectivity. *J. Appl. Meteor.*, **12**, 683-687.

Zawadzki, I. I., 1975: On radar-raingage comparison. *J. Appl. Meteor.*, **14**, 1430-1436.

Zawadzki, I. I., 1987: Fractal structure and exponential decorrelation in rain. *J. Geophys. Res.*, **92**, 9586-9590.

Zawadzki, I. I., and C. U. Ro, 1978: Correlations between maximum rate of precipitation and mesoscale parameters. *J. Appl. Meteor.*, **17**, 1327-1334.